Solid fuel pneumatic conveying and its injection geometry in a pressurized entrained flow gasifier

By
Francis Kus

Thesis submitted to the Faculty of Graduate and Postdoctoral Studies
In partial fulfillment of the requirements for the degree of M.A.Sc in Chemical Engineering

Department of Chemical and Biological Engineering
University of Ottawa
January 2016

© Francis Kus, Ottawa, Canada 2016

Abstract

Rising global energy demands have led to an increase in demand for clean, sustainable energy. A leading technology for reducing greenhouse gas (GHG) emission for existing coal-power infrastructure is gasification, which has sparked an interest in reactor modelling for design and performance analysis. Reduced order models (ROMs) have seen an increase in popularity for entrained flow gasifiers, as they offer a low-computational alternative to conventional computational fluid dynamic (CFD) modelling while maintaining the integrity of important operational parameters, such as carbon conversion and syngas yield. However, ROMs require more physical parameter inputs than are normally required for CFD modelling, such as the geometry of the gas-solid jet (specifically the jet half-angle).

Experiments were conducted to understand the relation between the required input parameters for ROMs, such as fuel flow rate, transport gas flow rate, and jet half-angle, and develop useful correlations for ROM systems. A new configuration for pneumatic conveying was developed and tested at the pilot-scale system at NRCan CanmetENERGY. It was used to study the pneumatic conveying of pulverized fuels, specifically the influence of operating parameters such as pressure drop and gas flow rates on the fuel flow rate, and the geometry of the gas-solid fuel jet (notably the jet half-angle) injected into the gasifier. The mean fuel flow rate of pulverized fuels was shown to increase with increasing pressure drop and with decreasing gas flow rates in the fuel transfer line. The jet half-angle was shown to increase as the solid loading ratio in the jet core was decreased. Finally, the relative fuel flow variability was observed to be significantly influenced by the design of the pneumatic conveying system, with the fluctuations increasing with increasing pressure drop and with decreasing gas flow rate, similar to the mean flow rate.

Sommaire

La hausse de la demande mondiale d'énergie a menée à une augmentation des besoins pour l'énergie propre et durable. Une technologie de pointe pour réduire les gaz à effet de serre provenant de la production d'électricité à partir du charbon est la gazéification, qui suscite un intérêt dans la modélisation du réacteur pour la conception et l'analyse de la performance. Les modèles d'ordre réduit (MOR) offre une alternative moins exigeante que la mécanique des fluides numérique tout en maintenant l'intégrité des paramètres importants tels que la conversion et le rendement. Bien que les MOR ont besoin de moins de temps pour compléter les calculs, ils requièrent plus d'information (e.g., demi-angle du jet gaz-solide) pour effectuer leurs tâches.

Des expériences ont été complétées afin de mieux comprendre la relation entre les paramètres requis pour les MORs (e.g., débit de combustibles, débit de gaz de transport, demi-angle du jet), et pour développer des corrélations pour l'utilisation des MOR. Une nouvelle configuration pour le transport pneumatique des combustibles a été développée à CanmetÉNERGIE, et a été utilisée pour étudier la relation entre les paramètres qui influencent le transport de solides (e.g., la différence de pression et le flux de gaz) et la géométrie du jet. Le flux moyen de combustible augmente lorsque la différence de pression à travers la ligne the transport augmente, ainsi que lorsque le flux de gaz de transport dans la ligne de transport diminue. Le demi-angle du jet augmente quand la concentration de solides dans le jet chute. Finalement, la variabilité du flux de combustible dépend grandement sur la géométrie du système de transport. Les fluctuations augmentent avec une plus grande différence de pression et un plus petit flux de gaz dans la ligne de transport.

Acknowledgements

I would like to express my sincere gratitude to my co-supervisors, Dr Poupak Mehrani and Dr Arturo Macchi, for their guidance and support throughout my undergraduate and graduate studies. Their experience and knowledge helped me a great deal during my time at the University of Ottawa.

I would also like to thank Dr Robin Hughes and Dr Marc Duchesne from CanmetENERGY for giving me the opportunity to work in the gasifier pilot plant, and for providing the equipment and expertise to perform the experiments that were required of me. Their help and knowledge is greatly appreciated. I would also like to extend my gratitude to Scott Champagne and Dr Dennis Lu for their frequent support and counsel during my stay. Additionally, I would like to thank the technical support staff at CanmetENERGY for their assistance in setup and operation of all the experiments undertaken.

Lastly, I would like to express my gratitude to my family and friends, for their support and patience during my studies.

Statement of Contribution of Collaborators

I am the sole author of all the chapters of this thesis. My supervisors, Dr Poupak Mehrani and Dr Arturo Macchi of the Department of Chemical and Biological Engineering provided editorial comments and supervised my work.

Chapter 2 is an article which was published in Powder Technology in 2016. This article was written by me, and was a collaboration with CanmetENERGY, Natural Resources Canada. Dr Robin Hughes and Dr Marc Duchesne provided editorial corrections and supervised my work at CanmetENERGY's research facilities.

Table of Contents

List of Figures

List of Tables

1. Introduction

International economic growth and development is leading to an increase in worldwide energy consumption. In 2012, 82% of global energy production was based on fossil fuels such as coal, petroleum, and natural gas [1] due to their high energy density and availability. The widespread use of fossil fuels for energy production necessitates the development of technologies capable of offsetting the substantial greenhouse gas (GHG) emissions.

Gases that are classified as known GHG contributors are carbon dioxide, methane, nitrous oxide, and chlorofluorocarbons [2]. CO_2 is an abundant by-product of thermochemical conversion processes to convert fossil fuels into usable energy, and as such its emissions from fossil fuel combustion have seen an exponential increase over the last 100 years, up to 32 $GtCO_2$ recorded in 2012 [1]. It has become an international priority to reduce GHG emissions from all sources, in order to limit the environmental footprint of society and mitigate further effects of climate change [3].

Many technologies have emerged over the past decade to aid in the reduction of GHG emissions from fossil-fuel power production (i.e. coal-fired power plants), which broadly fall into three categories: post-combustion, oxy-fuel combustion, and pre-combustion technologies [4]. In post-combustion carbon-capture, carbon is removed from the flue-gas and sent to storage. The removal of carbon can be done in a number of different ways, ranging from chemical (CaO) looping, to adsorption, to membrane separation [5]. Oxy-fuel combustion consists of reacting the fuel with pure oxygen, as opposed to air. In this process, the flue gas has a high concentration of CO_2, which can be easily recovered by condensing water [6]. The third technology, pre-combustion carbon separation is achieved by reacting the fuel under reducing conditions – a process known as gasification. The product gas is a mixture of carbon monoxide and hydrogen,

known as synthesis gas or syngas – other impurities such as ammonia, chlorine, and sulfur are removed in a gas treatment section prior to the clean syngas moving on to a gas turbine in which combustion takes place [4]. The gasification process is the key element to pre-combustion carbon separation, and will be discussed further in this thesis.

1.1 Gasification Process

Gasification is a thermochemical process in which a carbonaceous fuel, such as coal, petroleum coke, or biomass, reacts with oxygen in a reducing environment to produce syngas. Like any reaction, the composition of the product gas is highly dependent on the conditions at which gasification takes place. The temperature, pressure, and fuel-to-oxygen ratio fed to the reactor influence the carbon conversion and product yield. Additionally, there exist different types of gasification which will influence the limits of the achievable operational parameters: fixed bed (sometimes referred to as moving bed), fluidized bed, and entrained flow gasification [7].

There are many thermochemical reactions that occur during the gasification process. The reactions are often summarized as an overall reaction representing the gasification process (Reaction 1-1). Other important reactions that are often studied are the Boudouard reaction (Reaction 1-2), the methanation reaction (Reaction 1-3), the water-gas shift reaction (Reaction 1-4), and the steam methane reforming reaction (Reaction 1-5). For a detailed analysis on all reactions participating in the gasification process, the reader is deferred to Chapters 2 and 3 of Higman and Burgt [7].

$$C_nH_m + \frac{n}{2}O_2 \rightarrow n\,CO + \frac{m}{2}\,H_2 \qquad \text{Reaction 1-1}$$

$$C + CO_2 \leftrightarrows 2\,CO \qquad \text{Reaction 1-2}$$

$$C + 2\,H_2 \leftrightarrows CH_4 \qquad \text{Reaction 1-3}$$

$$CO + H_2O \leftrightarrows CO_2 + H_2 \qquad \text{Reaction 1-4}$$

$$CH_4 + H_2O \leftrightarrows CO + 3\,H_2 \qquad \text{Reaction 1-5}$$

Another reaction that is coupled with the gasification process is combustion (Reaction 1-6), where the solid fuel is converted to carbon dioxide and water. It is undesirable for combustion to dominate the reaction system, as the presence of carbon dioxide and water in the product gas reduces the heating value, and thus the thermal yield of the process. The fuel-to-oxygen ratio in the reactor is key to ensuring a high yield syngas – too much oxygen will result in a higher fraction of fuel combusting. Typically, a specific fuel-to-oxygen ratio will be determined for optimal gasifier performance, which depends on the fuel used.

$$C_nH_m + \left(n + \frac{m}{4}\right) O_2 \rightarrow n\,CO_2 + \frac{m}{2}\,H_2O \qquad \text{Reaction 1-6}$$

1.1.1 Fixed bed gasifiers

Fixed bed gasifiers consist of a vessel in which the fuel is deposited from a lock-hopper from the top of the vessel, and evenly distributed amongst the vessel's cross-section. The fuel undergoes multiple processes, including drying, pyrolysis, reduction (gasification) and oxidation (combustion). Ash or slag is removed at the bottom of the gasifier. There are two types of fixed bed gasifiers: updraft, in which the oxygen source (typically air) is introduced at the bottom of the reactor, and the syngas is collected at the top; and downdraft, in which the oxygen source is injected along the side of the reactor, below the pyrolysis region, and the syngas is collected near the bottom.

Figure 1-1 contains a schematic of updraft and downdraft fixed bed gasifiers. The combustion stage occurs first due to the excess oxygen in contact with the fuel. The reduction in oxygen in the gas phase causes the gasification stage to occur shortly after. The oxygen-depleted gas then proceeds to the pyrolysis stage, which is a thermochemical conversion of fuel to charcoal and tars in a high temperature (300-500 °C), oxygen-free environment.

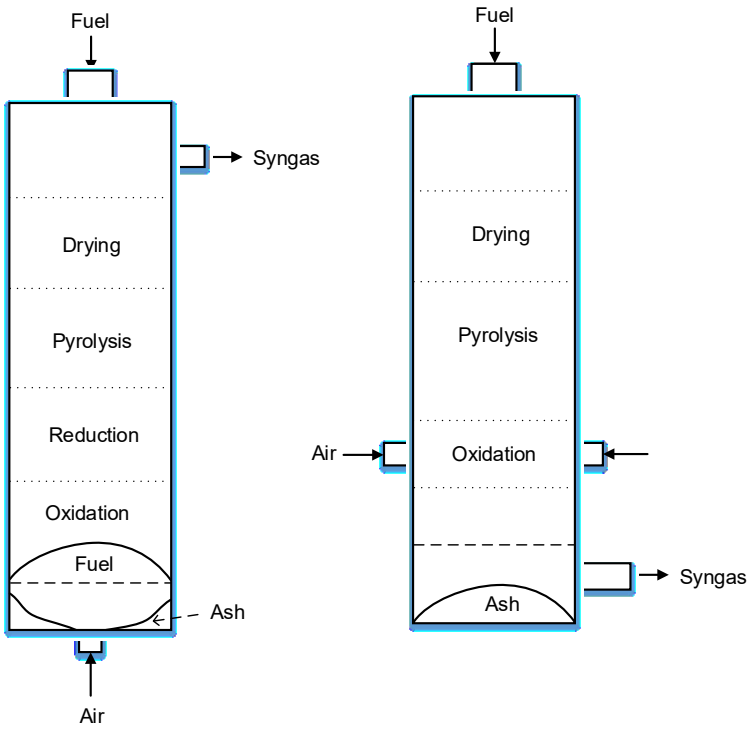

Figure 1-1: Simple schematic of fixed bed gasifier: updraft (left), downdraft (right)

Fixed bed gasifiers tend to have a high tolerance when it comes to feedstock variability. They can accept a wide range of particle sizes (it is recommended that fine particles smaller than 6 mm be avoided), as well as a wide variety of types of feedstock – various grades of coal, biomass, and even municipal solid waste are contenders for fixed-bed gasification. However, due to the lower reaction temperature (~800 °C), tar by-products and other by-products are typically found in the product gas, which calls for further treatment.

1.1.2 Fluidized bed gasifiers

In fluidized bed gasifiers, the fuel is fluidized in a mixture of oxygen and steam, where it is converted to syngas and ash. The elutriated particles are typically sent to a cyclone separation unit, where the syngas is removed, and the particles (ash or particles that have not completely reacted) are removed for further processing. A common application is the circulating fluidized bed (Figure 1-2), in which the particles are returned to the fluidized bed in order to increase overall conversion.

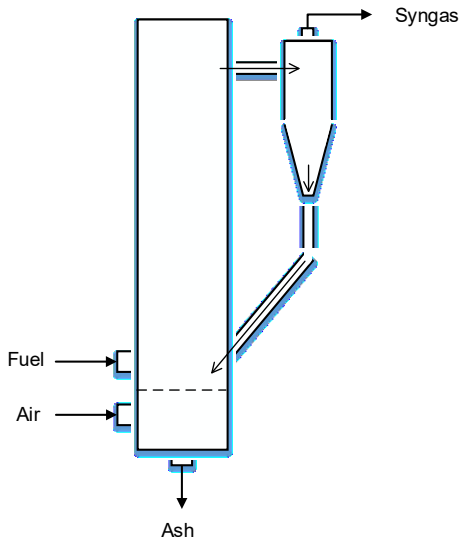

Figure 1-2: Simple schematic of a circulating fluidized bed gasifier

While fluidized bad gasifiers tend to have higher throughputs than fixed bed gasifiers, they come with their own operation challenges. Feedstock to the reactor must be limited in size (general < 10 mm), as fluidization of large particles can be difficult. Furthermore, due to the recirculation of ash into the fluidized bed, they cannot operate above the softening point of ash without causing particle agglomeration, which will reduce the reactivity of the fuel, and render the particles more difficult to fluidize. However, operating at lower temperatures means that syngas yield is reduced in the form of higher tar production, which is undesirable.

1.1.3 Entrained flow gasifiers

Entrained flow gasifiers consist of a vessel in which the fuel and oxygen are injected together, via a burner ensemble. The reaction temperature of this process is often in excess of 2000 °C, resulting in a high carbon conversion and syngas yield (no tar by-product). These high operating temperatures result in ash removed from the gasifier in the form of slag. However, the residence time of these types of reactors can be very short, as little as a few seconds [8]. As a result, feedstocks are limited to fine particles, in the range of 30 to 100 µm, to ensure complete conversion of the fuel before exiting the reactor. Figure 1-3 shows a schematic of an entrained flow slagging gasifier.

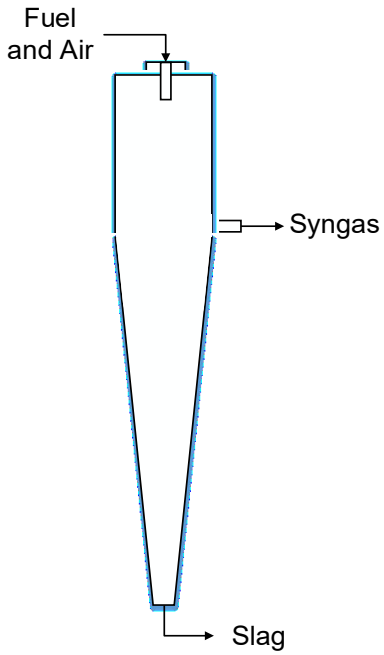

Figure 1-3: Simple schematic of an entrained flow gasifier

The low residence time of the reaction means that the product composition is sensitive to variations in fuel flow. Changes in the fuel-to-oxygen ratio fed to the reactor can lead to significant changes in temperature and product composition, as the reaction alternates between

gasification and combustion. This results in excess strain on the equipment, which can lead to significant burner damage and possibly flow disruption. Despite these operational concerns, entrained flow gasifiers tend to have a high fuel throughput, with high syngas yields [9] which makes them a strong competitor as a pre-combustion technology.

1.1.4 Gasification modelling

While gasification has been studied for several decades, the increasing demand for low emissions technology in recent years has increased interest in the technology. Most work on entrained flow gasification has focus on the reaction itself – studying the effects of temperature, pressure, fuel composition, and oxidizing agent. Kirubarakran *et al*. [10] provide a review work done on biomass gasification, analyzing the influence of parameters such as particle size and shape, to reactor temperature, heating rate, and medium. Brar *et al.* [11] review coal and biomass cogasification, summarizing the influence of different fuel mixture compositions on the product syngas composition, emphasizing the environmental benefits of the process. Murthy *et al.* [12] review existing gasification technologies and models, specifically for applications with petroleum coke (a by-product of the oil processing industry). They emphasize the importance of proper mathematical modelling of gasifiers in design and performance optimization.

Proper modelling of gasification is important for the understanding of reactor design and performance. Computational fluid dynamic (CFD) modelling is a powerful tool, as it includes detailed multi-phase sub-models of the gasification process, including reaction kinetics and solid-fluid momentum balances. However, the high computational requirement results in some undesirable side effects, namely the time required for convergence (a single gasification condition can take several days) [13]. An alternative is to use a reduced order model (ROM). ROMs are simplified models that are designed to reduce computational requirements, while

maintaining the integrity and accuracy of important characteristics, such as conversion, temperature profiles, and product composition. However, they require more user-defined physical parameters, such as the jet geometry, that are otherwise determined by the equations of state used in a CFD model.

The reduced complexity of ROMs allows for computation of transient behaviour of a gasification system. Provided proper transient input models (such as the fuel flow rate over time), the corresponding transient behaviour of the reactor can be modelled (such as conversion and yield over time).

1.1.5 Pneumatic conveying for gasification

An efficient gasification system is dependent on a reliable flow of fuel from a supply hopper, as the quality of the syngas will suffer if the fuel-to-oxygen level cannot be maintained. The design and operation of gasifiers require knowledge of the conveying characteristics of the fuels that are used. The challenge behind the conveying of fuels in gasification systems is the wide variability in fuel properties. Typical fuels are coal, petroleum coke, and biomass (in the form of forestry waste, or fine sawdust). For entrained flow gasification, the particles size needs to be small enough such that complete conversion can occur within the short residence time. The fuels are generally pulverized to sizes under 100 μm. However, the particle shape and size distributions result in operational challenges such as fuel consolidation, plugging, channeling, and a high variability in fuel flow.

Some work has been done on the modelling of pneumatic transport of pulverized coal [14–18]. Information on the transport characteristics of petroleum coke and biomass is lacking. It is of interest to understand the influence of conveying operating parameters (such as pressure drop

and transport gas flow rates) on the flow of these fuels in pneumatic conveying systems, and to develop pneumatic conveying models that can be applied to ROMs.

1.1.6 The jet half-angle

As mentioned in section 1.1.4, ROMs require additional physical property inputs that CFD models do not require; notable the fuel jet half-angle (shown in Figure 1-4). The jet half-angle was shown to have a significant impact on the gasifier fuel conversion and yield predicted by the ROM – variations as small is 1° in the half-angle can have a significant impact on the predicted gasification performance, for instance the carbon conversion was shown to change by up to 1% [19,20]. Jet half-angles for gas-solid systems such as entrained flow gasifiers have been shown to be influenced by the solid loading ratio of the jet [21,22] (the solid loading ratio defined as the mass flow rate of solids over the mass flow rate of transport fluid, in this case the transport gas). However, jet half-angle modelling is limited to liquid and gas jets. In a similar fashion to the pneumatic conveying of fuels, it is of interest to determine the jet half-angle behaviour for different operating conditions, such as gas and fuel flow rates, and develop jet half-angle models for gas-solid jets that can be applied to ROMs.

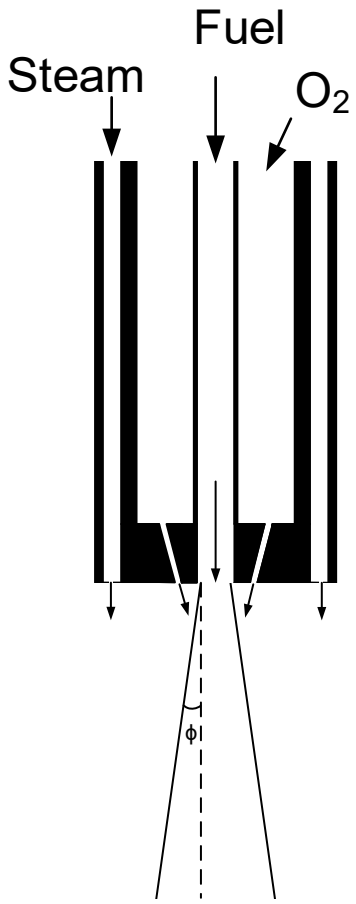

Figure 1-4: Gasifier burner tip, demonstrating the different flow channels of the reactants in an entrained flow gasifier, as well as the jet formed (ϕ indicates the jet half-angle).

1.2 Thesis Objectives

The objective of this thesis was to study the fuel conveying characteristics associated with entrained flow gasification, and their influence on physical properties required for reduced order modelling, notably the mean fuel flow rate, the fuel flow rate variability, and the jet half-angle in the gasifier. The pilot-plant gasification system at CanmetENERGY, Ottawa, Canada was used to achieve these goals. The specific goals were as follows:

- Develop and test a pneumatic conveying feed system configuration from which pulverized fuels (lignite, petroleum coke, and biomass) can be reliably conveyed to an entrained flow gasifier.
- Determine the influence of pneumatic conveying operating parameters (pressure drop, transport gas flow rates, transport gas injection point) on the fuel flow rate.
- Determine a mathematical model for pneumatic conveying of pulverized fuels to predict solid fuel flow rate for use in reduced order models.
- Determine the influence of pneumatic conveying operating parameters (solid loading ratio) on fuel jet geometry for use in reduced order models.
- Determine a mathematical model for the jet half-angle for use in reduced order models.
- Determine the fuel flow variability of a pneumatic conveying system, and develop a mathematical model for use in reduced order models.

The chapters within this thesis investigate the above objectives, and provide additional in depth background on each topic (fuel conveying, jet geometry, and fuel variability study).

1.3 Thesis Outline

The thesis is divided into five chapters from which two chapters are prepared as journal publications. Chapter 2, entitled "*Pressurized pneumatic conveying of pulverized fuels for entrained flow gasification*", highlights the development and testing of a new fuel pneumatic conveying system for an entrained flow gasifier, investigates the influence of the operating parameters on the fuel flow rate, and presents a mathematical model for the pneumatic conveying of pulverized fuels. This chapter is prepared in a journal manuscript format and is published in the journal *Powder Technology (2016, 287, 403-411)*.

Chapter 3, entitled "*Jet half-angle measurements and correlation for an entrained flow gasifier*", investigates the jet half-angle of a solid-loaded jet, determines the impact of the conveying operating parameters (solid loading ratio), and presents a mathematical model for the jet half-angle. This chapter is prepared in a journal manuscript format and will be submitted to the journal *Powder Technology*.

Chapter 4, entitled "*Frequency analysis of a pneumatic conveying system*", investigates the variability of the fuel flow in the pneumatic conveying system described in Chapter 2, and provides a mathematical model for the fluctuations observed.

Chapter 5 presents the overall conclusions of this research and recommendations for future investigation.

2. Pressurized pneumatic conveying of pulverized fuels for entrained flow gasification

FT Kus[ab], MA Duchesne[b], S Champagne[b], RW Hughes[b], DY Lu[b], A Macchi[a], P Mehrani[a*]

[a] Department of Chemical and Biological Engineering, University of Ottawa

161 Louis Pasteur Street, Ottawa, Canada, K1N 6N5

[b] Natural Resources Canada, CanmetENERGY

1 Haanel Drive, Ottawa, Canada, K1A 1M1

Article published in *Powder Technology* **2016** *287*, 403-411

2.1 Abstract

A pneumatic conveying system has been designed for the continuous conveying of pulverized fuels, namely biomass (in the form of Canadian forestry waste), lignite, and petroleum coke, to an entrained flow gasification unit. All three fuels studied exhibit properties that are challenging for fluidization or conveying. The lignite and petroleum coke are Geldart class C particles and are expected to exhibit difficulties in conveying, while the biomass is a Geldart class A particle but the non-uniform particle shape and large size distribution result in pneumatic conveying challenges similar to class C particles. The conveying system consists of a blow vessel with three points of gas injection to aerate the bed of material and facilitate hopper discharge. The mass flux of each material was studied as the system parameters were varied, which included: fluidizing and sparge gas (two of the three gases aerating the hopper bed), transfer gas (gas injected directly into the solid transfer line), pressure drop, conveying gas type and transfer line diameter. Fuel fluxes were varied in a range of 450 kg/m^{2}s to 1700 kg/m^{2}s for all three fuels. Compared to lignite and petroleum coke conveying, biomass conveying was found to have a smaller gain in mass flux to many conveying parameters investigated. Additionally, several models for pneumatic conveying of powders were compared against the data obtained. The models were found to have various degrees of relative error, with the best fitting model having a relative error of less than 10% for all three fuels with a marginal bias towards underestimation.

2.2 Introduction

Gasification consists of the conversion of carbonaceous fuels into carbon monoxide and hydrogen; a mixture known as syngas, which has many uses in the energy and chemical industries. The quality of the syngas produced is dependent on its composition, as carbon dioxide and steam can also be produced. The production of these by-products is caused by combustion

occurring in the gasifier reaction chamber, due to a reduction in the carbon-to-oxygen ratio. In order to maximize the calorific value of the syngas, the carbon-to-oxygen ratio needs to remain at a constant value that is dependent on the oxygen source and fuel [23]. This relationship is emphasized in low residence time processes, such as downdraft entrained flow gasification, where the residence time can be only a few seconds [8].

An advantage of gasification is the wide range of fuels that can be used as a carbon source. Coal is an abundant resource and is typically used in gasification processes [23], but fuels such as petroleum coke and biomass have important implications as well [8]. Petroleum coke is a by-product of the oil processing industry, and is being produced in increasing quantities due to increased oil demand [24,25]. Biomass, on the other hand, is being considered as an alternative to fossil fuels, and a source for reducing CO_2 emissions [24].

The pneumatic conveying of pulverized solids has an important role in the gasification process, as the quality of the syngas is dependent on a reliable flow rate of solid fuel into the gasifier. Thus, the flow characteristics of solid fuels through conveying lines are important for both design and operation of gasification plants. Design procedures for pneumatic conveying systems are well defined for free-flowing particles of uniform shape and size [26,27]. However, particles that are not in accordance with these criteria tend to be more difficult to convey.

Some work has been done over the years on modeling and optimizing pneumatic transport of fuels, namely pulverized coal. Sprouse and Schuman [14] have developed a model to determine solid and gas flow from a conical hopper, resulting from the momentum balance of both solid and gas phases. Geldart and Ling [15] defined the total pressure drop along a solid-gas transport line as the summation of various contributing factors (particle acceleration, bends, static head, solid friction, and gas friction), while determining the friction factor of solids through a transfer

line is the focus of other studies [16,17]. Huang *et al*. [18] studied the discharge of cohesive coal particles from a blow vessel, and determined that conventional designs are inadequate: aerating the material in the hopper is required to achieve continuous flow of cohesive material from a hopper.

Conventional fuels, such as pulverized coal, have received much of the focus on pneumatic conveying research due to their historical prevalence. Conversely, the conveying characteristics of fuels such as petroleum coke and biomass have received little attention. Most work involved with the use of biomass as a fuel source has been on the thermochemical conversion itself (such as gasification, combustion, and pyrolysis technologies). Little research has been done on the pneumatic conveying characteristic of biomass, which is problematic for technology that may rely on biomass as a feed source. The fibrous nature and broad particle size distribution of the material translates to poor fluidization, leading to challenges in conventional pneumatic transport systems [28]. These issues can range from particle segregation, causing larger particles to form plugs in the transport line as they are not conveyed, to material consolidation causing plugs at the location of discharge from the feed hopper.

The objectives of this research involve determining a feed system configuration from which pulverized fibrous biomass can be conveyed continuously. In addition, the influence of the system parameters (such as pressure drop, gas flow rate, and gas injection point) on the mean mass flow rate of the fuel is determined for biomass, petroleum coke, and lignite, using the same system developed for the biomass. Finally, results obtained are compared with several existing models for pneumatic conveying of powders.

2.3 Fuel Analysis

The pneumatic conveying characteristics of three different pulverized fuels were studied herein: biomass (in the form of residual forestry waste, or sawdust), lignite, and petroleum coke. Fuel properties analyzed include particle shape, density, and mean size. An overview of these properties (Table 2-1) provides insight as to the unique challenges faced when attempting pneumatic conveying of these particles.

Table 2-1: Overview of fuel physical properties

Fuel	Shape	Particle Density, ρ_s	Particle Size, $d_{Harmonic}$	Geldart Classification
Biomass	Fibrous	947 kg/m^3	60 µm	A
Lignite	Polyhedral	907 kg/m^3	11 µm	C
Petroleum Coke	Polyhedral	1176 kg/m^3	10 µm	C

The particle shape was analyzed using a scanning electron microscope (SEM). The results are illustrated in Figure 2-1. Lignite and petroleum coke are polyhedral, whereas the biomass consists of elongated, fibrous shapes. This is an important consideration in fluidization and conveying of particles – the fibrous structure of the biomass contributes to the challenges in conveying and fluidizing this material [28].

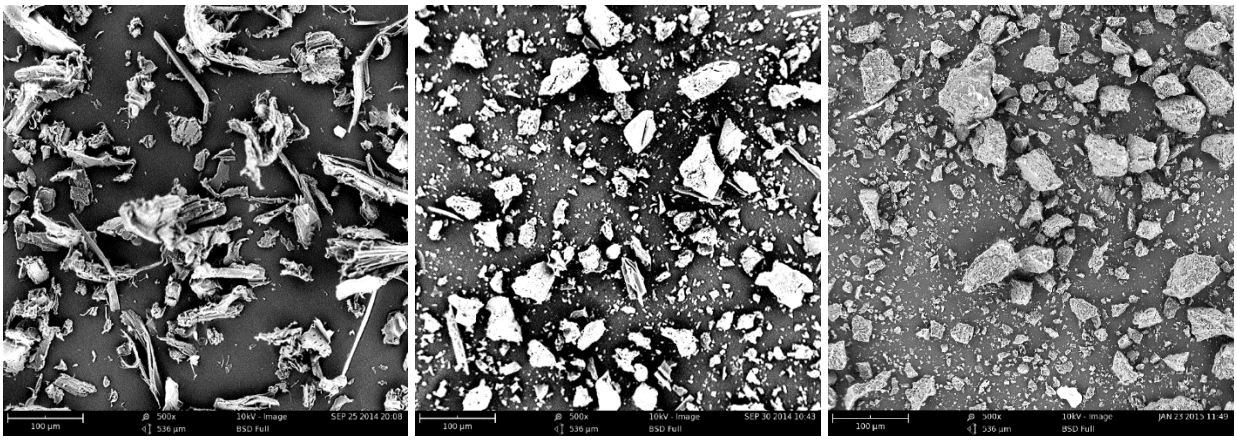

(a) *(b)* *(c)*

Figure 2-1: SEM images of the pulverized fuels: a) biomass; b) lignite; c) petroleum coke

The particle size distribution for all three fuels was determined using a *Microtrac LT-100* laser diffraction particle size analyzer, which provides the size distribution on a volume basis. The size distributions are found in Figure 2-2. It is of note that the lignite and petroleum coke have very similar particle size distributions. The harmonic mean of the volume distribution, seen in Equation 2-1, was determined for each fuel. The particle density (ρ_s) was measured using mercury pycnometry.

$$d_{Harmonic} = \frac{1}{\sum \frac{1}{x_i d_i}} \qquad \text{Equation 2-1}$$

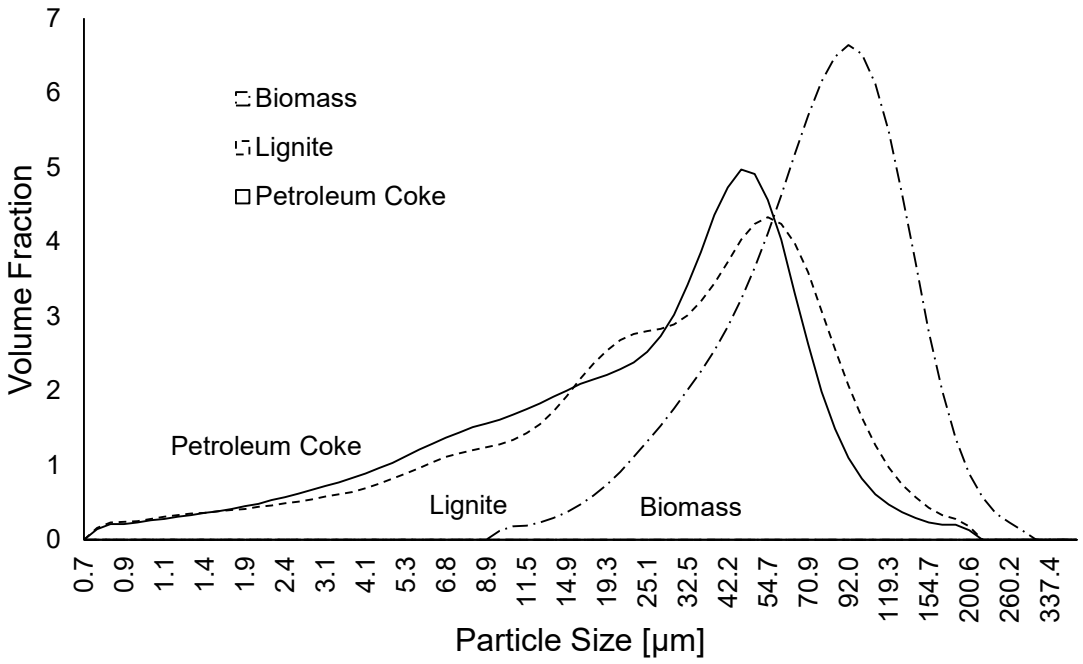

Figure 2-2: Particle size distribution of pulverized fuels, determined using a Microtac LT-100 particle size analyzer

The ease at which a fine powdered material can be handled depends on the fluidization characteristics of the material, defined by Geldart's powder classification [29]. The classes consist of four groups: A, B, C, and D, and can be estimated using particle properties (density and particle size). Most work on pneumatic conveying of fines is performed on type A powders, as they are the ideal candidates for fluidization. The Geldart classification of the three fuels can be found in Table 2-1, along with an overview of the other particle properties analyzed. Biomass is classified as "easily fluidizable", whereas the lignite and petroleum coke are classified as "cohesive" and should not exhibit good fluidization. It should be noted that this is not the only requirement for proper fluidization.

2.4 Experimental Setup

The dense-phase conveying system in the gasification pilot plant at Natural Resources Canada, CanmetENERGY (Ottawa, ON, Canada), was used to determine flow characteristics of the three fuels. The system was refit for non-reactive testing by conveying the fuel into a second hopper in place of the gasifier. The system consists of two identical hoppers, where the fuel is conveyed from the bottom of the first hopper (the feeder, or feed hopper) to the top of the second hopper (the receiver, or receiver hopper). The receiver is held at a constant pressure of 1600 kPa, while the feeder pressure can be adjusted to achieve the desired pressure drop across the conveying system. It should also be noted that while many pneumatic conveying analyses (particularly modelling) focus on either horizontal or vertical conveying, this system is composed of a combination of both: two horizontal sections (4.4 meters total) and two vertical sections (10.5 meters total).

2.4.1 Feed hopper design

The configuration of the feed hopper has a significant impact on the flowability of the fuels studied. The configuration selected must be able to discharge material from the hopper at a continuous rate in order to demonstrate the viability of the system for industrial use. Given the difficult nature of conveying pulverized biomass, a functional configuration for conveying the biomass was first determined and consequently adopted for all other fuels. Hopper design for pneumatic conveying systems is detailed by Klinzing *et al*. [26] and Mills [27]. For a high pressure system conveying fine, cohesive material, it is recommended to use a blow vessel with minimal moving parts. Studies using irregular shaped particles with wide size distributions indicate that irregular shaped particles, or broader particle size distributions, are more likely to cause blockages using mechanical equipment such as screw conveyers [30]. Despite the

conveying design guidelines put into place, several hopper variants (see Figure 2-3) were attempted prior to the adoption of a final functioning configuration.

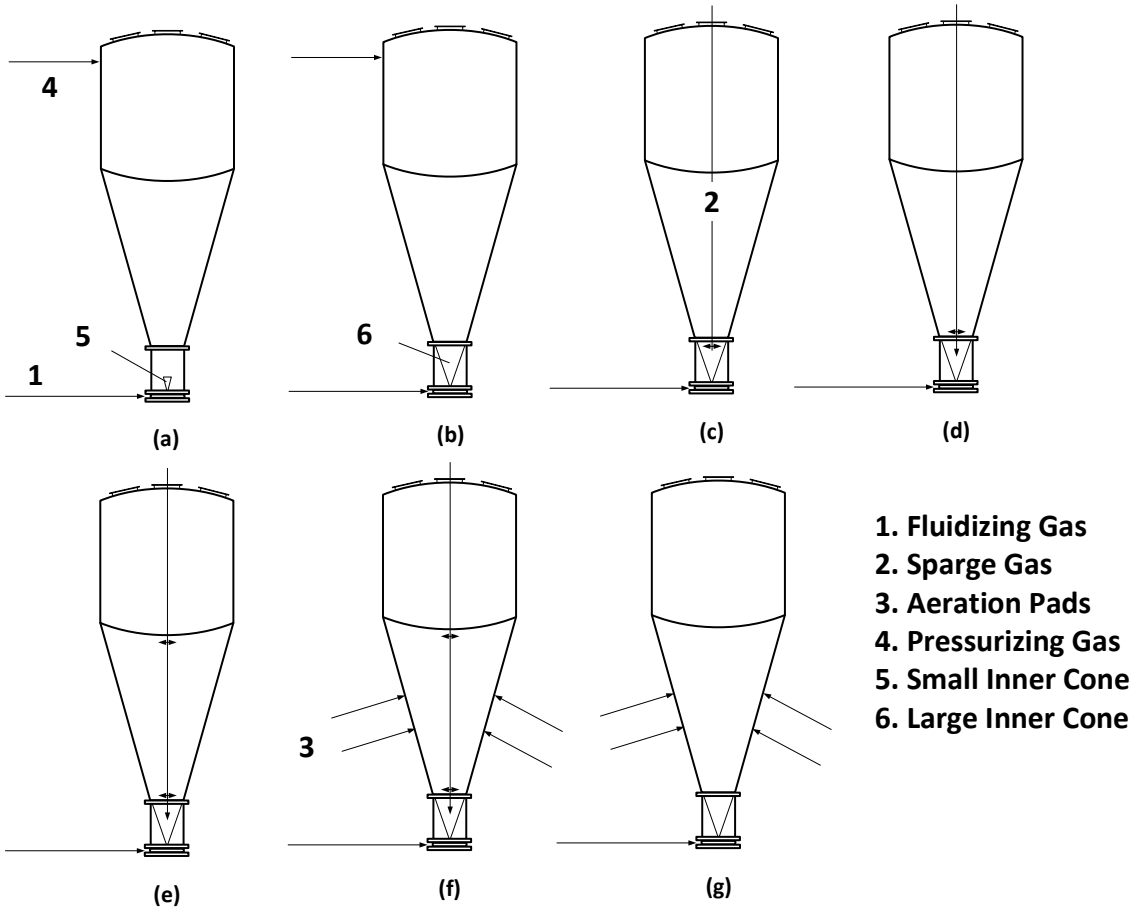

Figure 2-3: Schematic of various hopper configurations tested for pulverized biomass conveying; (a) initial hopper design (b) extension of inner cone for smooth transition (c) addition of sparge tube (d) modification of sparge tube (e) second modification of sparge tube (f) addition of aeration pads (g) removal of sparge tube to observe influence of aeration pads

A high pressure blow vessel was used as the feed hopper, charged with supplying material to the conveying line. The initial configuration was pressurized from the top of the hopper and contained a small cone (38 mm diameter) at the bottom of the vessel to facilitate the transition from the hopper outlet to the transfer line (a). This was later expanded to a larger cone in order to have a continuous gradient from the hopper into the transfer line (b), corresponding to a size

reduction from 10.16 cm to 0.77 cm. Further plugging and channeling in the vessel led to systematic configuration modifications that resulted in the inclusion of a fluidizing ring, a sparge tube and aeration pads (c-f) that served to aerate the bottom cone in the vessel and allow for continuous fuel discharge from the hopper. A detailed schematic of the final hopper configuration is shown in Figure 2-4.

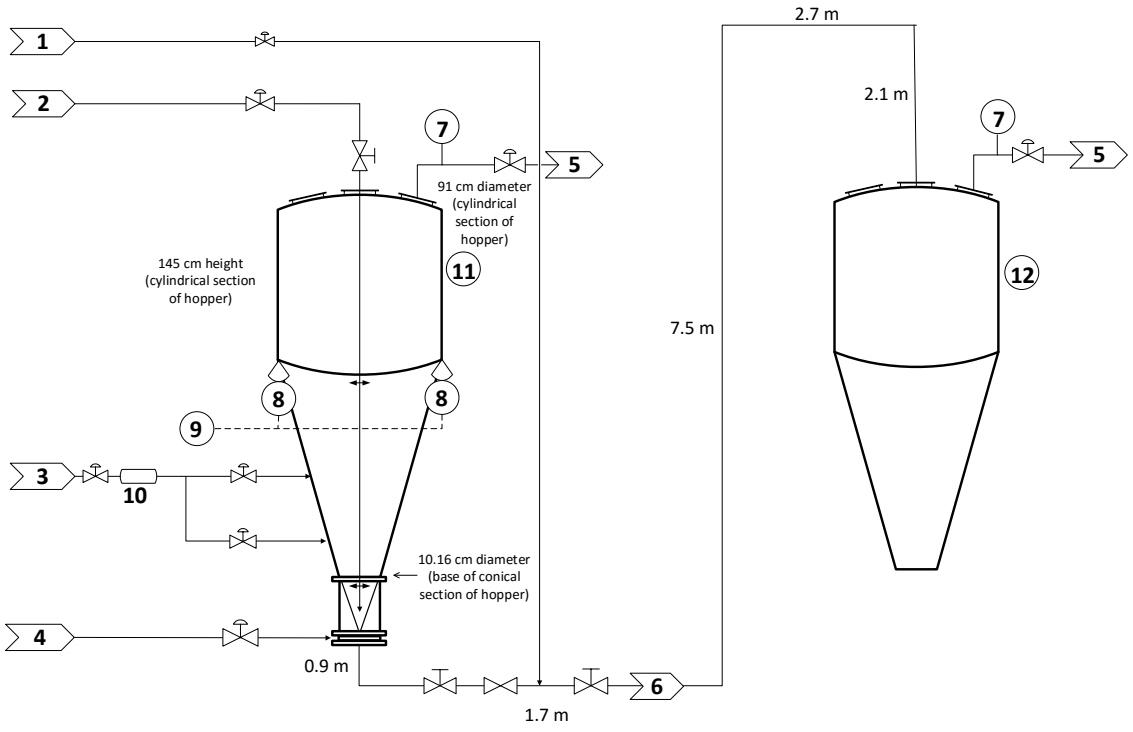

Figure 2-4: Configuration of feed hopper in the cold-flow dense-phase conveying system at Natural Resources Canada, CanmetENERGY. 1) Transfer gas; 2) Sparge gas; 3) Aeration pad; 4) Fluidizing gas; 5) Hopper vent; 6) Transfer line to receiver; 7) Feed vessel pressure gauge; 8) Feed vessel scale; 9) Feed vessel weight differential; 10) Surge vessel; 11) Feed vessel; 12) Receiver vessel

The hopper is constructed of 316 stainless steel and has a half angle of 15°, consistent with previous powder conveying studies [14,15]. The inner diameter of the cylindrical section of the hopper measures 91 cm (wall thickness of 0.95 cm), and decreases to a 10.16 cm opening at the

base of the conical section where it transitions to a 0.95 cm OD stainless steel tube. The tube is then reduced as necessary to the desired line size (0.46 cm, 0.61 cm, and 0.77 cm ID). The volume of the hopper is 1.2 m^3, resulting in maximum hopper inventories of approximately 250 kg for biomass, and 500 kg for petroleum coke and lignite. This difference in bed inventory is due to the larger bed porosity of the biomass, resulting in a much lower bulk density.

The conveying gas is introduced into the system via four pathways: fluidizing gas, sparge gas, transfer gas, and aeration pads. The fluidizing gas serves to prevent material packing upon pressurization, and consists of gas introduced via a fluidizing ring at the bottom of the hopper. The sparge gas serves to prevent material from bridging at the discharge point in the cone, and is introduced via a 'sparge tube' that is injected through the center of the bed of material to the bottom of the hopper. The sparge tube consists of a 0.46 cm tube that injects gas into the feed hopper at three locations via 0.1 cm holes: at the end of the sparge tube in a downward direction, just above the cap in two positions at 180º increments around the tube, and another 30.5 cm higher on the sparge tube in four positions at 90º increments around the tube. A vent is used to maintain constant pressure in the hopper as gas flow rates are varied.

The transfer gas is injected directly into the solid fuel transfer line, and serves as the primary source for controlling the transport gas in the line. The aeration pads pulsate gas into the hopper on a one-minute cycle: a surge tank fills with gas at high pressure (2300 – 2500 kPa) for 50 seconds, and discharges into the hopper over a 10 second period, alternating between 3 pads in a higher position in the vessel and 3 pads in a lower position (see Figure 2-4). This action serves to prevent channeling from occurring by breaking any consolidated structures that may have formed within the hopper.

2.4.2 Experimental conditions

The influence of several system parameters on the mean flow of solid fuel was studied in order to analyze the fuel flow characteristics. The range of operating parameters tested is summarized in Table 2-2. It includes the upper and lower limits studied for the system parameter indicated, using each fuel.

The parameters studied include the bed inventory (quantity of solid fuel in the hopper), the transfer line outer diameter, the pressure drop between the feed hopper and receiving hopper, the injected gas flow rates (i.e., fluidizing gas, sparge gas and transfer gas flow rates), and the carrier fluid (nitrogen and carbon dioxide). Some parameters were chosen as a basis of comparison between the work conducted and previous work (e.g., pressure drop, line diameter, and transfer gas), while others are particular to the system under study (e.g., fluidizing gas and sparge gas flow rates). For all results presented in this article, the carrier fluid is nitrogen, unless otherwise specified.

Table 2-2: Range of operating parameters studied

System Parameter	Biomass	Lignite	Petroleum Coke
Bed Inventory (kg)	70-200	170-260	60-470
Transfer Line Inner Diameter (cm)	0.61, 0.77	0.46, 0.61	0.46
Pressure Drop (kPa)	75-240	100-220	80-220
Fluidizing Gas Flow (kg/h)	6-15	1-12	1-12
Sparge Gas Flow (kg/h)	6-15	1-12	1-12
Transfer Gas Flow (kg/h)	1-3	1-8	1-5
Carrier Fluid	N_2	N_2, CO_2	N_2

The fuel flow from the hopper is measured using load cells, which measure the change in mass over the preceding 30 seconds, and use this value to calculate the flow of material from the hopper [kg/h]. A moving average function is used. The mean flow rates and their standard deviations are calculated over a run period of ten minutes per condition, where an average run period of 5 hours per day was achieved. The figures reported contain these mean values, and the error bars represent the standard deviation of flow within a run.

2.5 Data Analysis

2.5.1 Effect of bed inventory on solid flux

The mean solid flux of each fuel was determined at identical conditions for varying hopper inventory to determine the effect of the mass of fuel in the hopper on the mean fuel flow. This was primarily a precaution to ensure that the results would not be dependent on the order they were obtained during a run. Figure 2-5 shows the solid flux of the fuel measured with different bed inventories. It can be seen that the solid flux is not dependent on the bed height; the variation with different bed inventories is smaller than the standard deviation for each test.

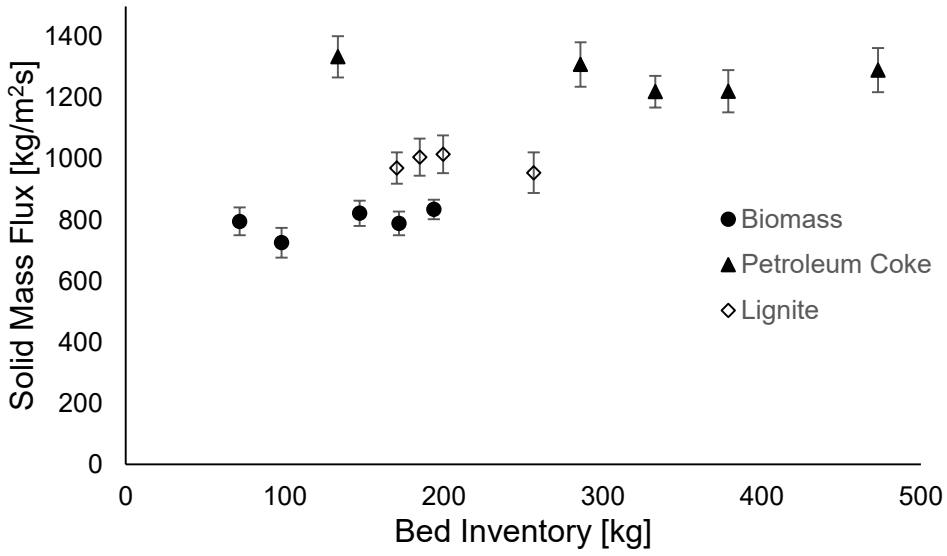

Figure 2-5: Solid flux of pulverized fuels at different bed heights, for constant conditions (sparge gas = 4 kg/h; fluidizing gas = 4 kg/h; transfer gas = 4 kg/h; pressure drop = 150 kPa; line diameter = 0.46 cm for lignite and petroleum coke, 0.61cm for biomass).

2.5.2 Effect of line diameter

The momentum balance analysis performed by Sprouse and Schuman [14] shows a proportional relationship between the mass flow of pulverized solids and the square of the diameter of the transfer line used. In alternative terms, the mass flux $\left(\frac{4m_s}{\pi D^2} = \bar{m}_s\right)$ is constant as the line diameter is varied. Figure 2-6 shows the biomass and lignite fuel flux as the pressure drop across the transfer line is increased with different line diameters and constant gas flow rates. The solid fluxes are similar when the line diameter is varied.

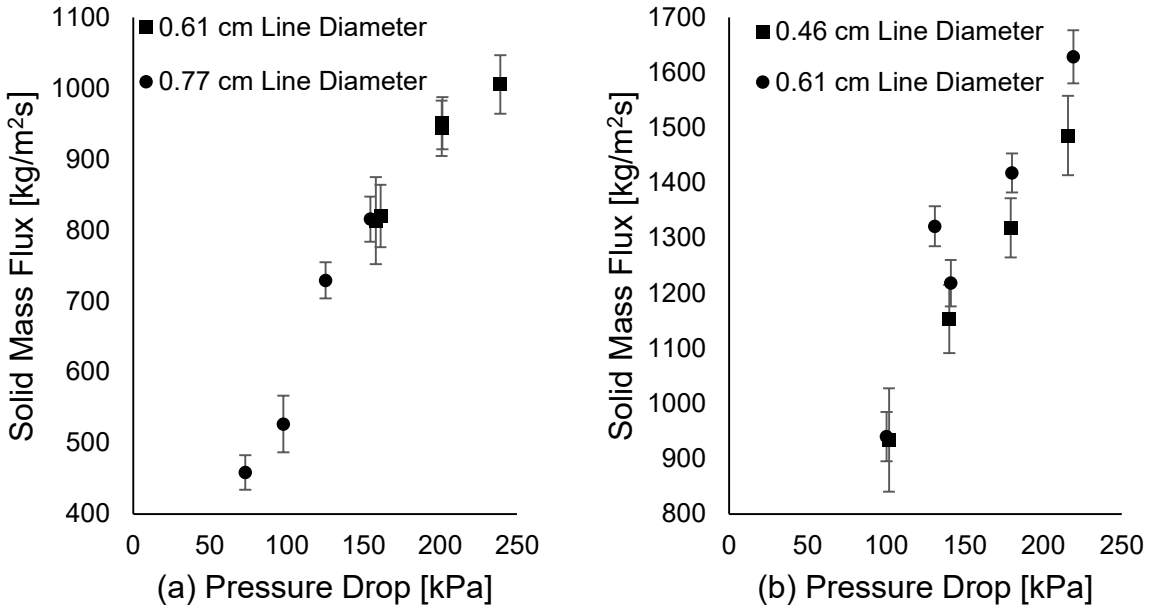

Figure 2-6: Fuel flux as pressure drop is varied at different line diameters for (a) biomass and (b) lignite, for constant gas flow rates (biomass: fluidizing gas at 14 kg/h, sparge gas at 14 kg/h, transfer gas at 1 kg/h; lignite: fluidizing gas at 4 kg/h, sparge gas at 4 kg/h, transfer gas at 1 kg/h).

2.5.3 Effect of gas injection point

Flow rate from the three gas injection points (denoted as fluidizing gas, sparge gas, and transfer gas) were varied individually for all three fuels to study their effects while maintaining constant flow rates for the other two gas injection points and a constant system pressure drop. As shown in Figure 2-7, the fluidizing gas was found to have a negligible effect on the flux of all three fuels, whereas the sparge and the transfer gas had a noticeable impact on the flux of lignite and petroleum coke. An increase to either the sparge or transfer gas results in a decrease in the solid fuel flux, as the solid material in the transfer line becomes diluted with gas. The biomass flux is not significantly influenced by the gas flow rates, possibly a result of the higher compressibility

of the material. The increase in force acting upon the material in the conveying line (caused by an increased gas flow rate) could cause the material to compact, reducing the dilution effect.

With regards to the fuel flow variability, the standard deviation of the flux during a single ten-minute run is lower for the tests involving biomass, and the deviation does not vary significantly as any of the gas flow rates are changed. In contrast, higher sparge gas flow rates appear to increase the standard deviation of the fuel flux for lignite and petroleum coke.

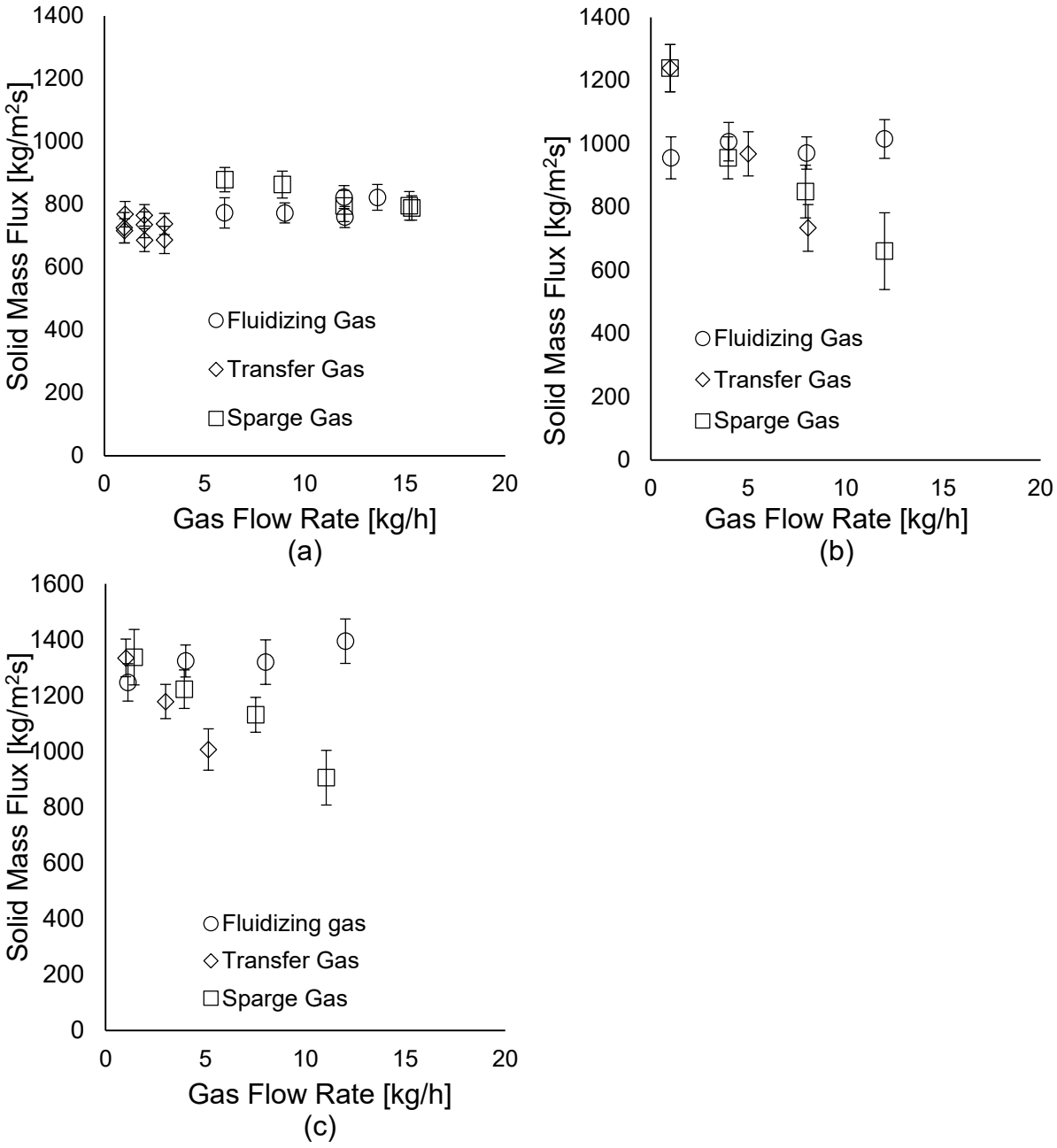

Figure 2-7: Effect of gas injection point for (a) biomass, fluidizing gas at 15 kg/h, sparge gas at 15 kg/h, transfer gas at 1 kg/h, line diameter of 0.61 cm; (b) lignite, fluidizing gas at 4 kg/h, sparge gas at 4 kg/h, transfer gas at 1 kg/h, line diameter of 0.46 cm; and (c) petroleum coke, fluidizing gas of 4 kg/h, sparge gas of 4 kg/h, transfer gas of 1 kg/h, line diameter of 0.46 cm; pressure drop of 150 kPa for all fuels

2.5.4 Effect of pressure drop

Figure 2-8 demonstrates a linear relationship between the solid flux of fuel and the pressure drop through the transfer line, which is in corroboration with a number of pneumatic conveying models [14,15,17]. It should be noted that the biomass flux is lower than that of lignite and petroleum coke for equivalent pressure drops, suggesting an increase in solids friction, resulting in lower flow rates of biomass. As shown previously particle mean size, size distribution and shape of lignite and petroleum coke are similar, whereas the biomass differs significantly (in both particle diameter and shape). In contrast, the fuel densities are different for all three fuels. The similarity of the fuel flow behaviour between the lignite and the petroleum coke, and the significant difference with the biomass, suggest the particle size distribution and shape have a significant impact on the mean fuel flow whereas the particle density offers a lesser contribution. In accordance with this observation, some conveying models do not include particle density, however they do contain empirically determined coefficients that are dependent on the material conveyed [15,17].

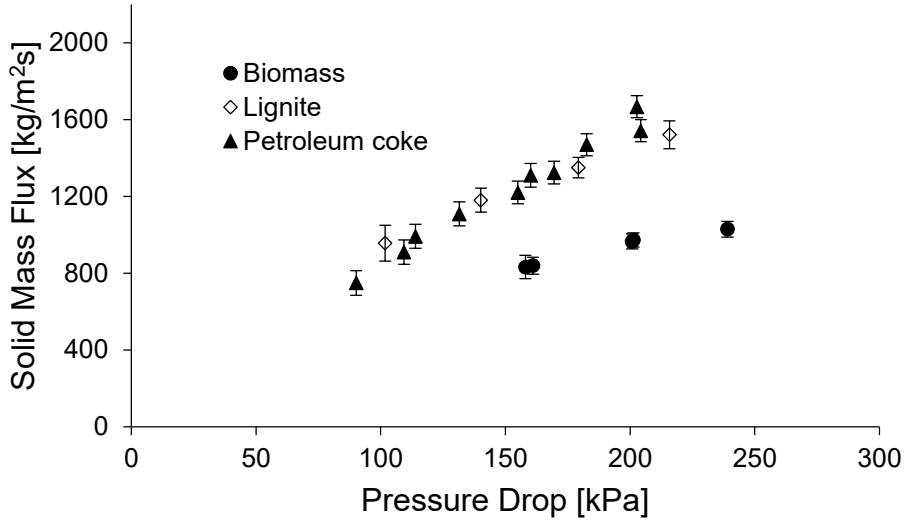

Figure 2-8: Fuel mass flux as pressure drop is varied, for biomass, lignite, and petroleum coke.

2.5.5 Effect of carrier fluid

Most of the published work on pneumatic conveying of fine particles focuses on air or nitrogen as carrier fluids, likely due to their accessibility and use in air-blown systems. As such, nitrogen was used for most experiments carried out in this study. However, fluid properties such as density are known to influence fluidization behaviour of powders, and are considered in the development of pneumatic conveying models [14–17]. There are practical benefits to using other carrier fluids, particularly in combustion or gasification applications. For instance, carbon dioxide is frequently used in gasification applications, as it reduces nitrogen dilution of the product gas [23,28].

The effect of carrier fluid density on fuel conveying was observed through comparison between nitrogen and carbon dioxide tests for conveying pulverized lignite. This effect is known to be complex, as there are many influential parameters that drive discharge of fuel from the hopper and the conveying of fuel in the transfer line. It is reported that CO_2 is less capable than air of

fluidizing powders due to its affinity to adsorb onto the fuel [31], however it was shown that the discharge of fuel from a hopper is both a function of the fluidization in the hopper and the effectiveness of the carrier fluid in the transfer line [32]. Due to the unique nature of the conveying system used (combination of fluidizing gas, sparge gas, and aeration pads in the hopper, and transfer gas injected directly into the transfer line), it is difficult to predict what effect the type of carrier fluid might have on the fuel flux. The experiments conducted show that the carrier fluid does not have an observable effect on the fuel flux (Figure 2-9).

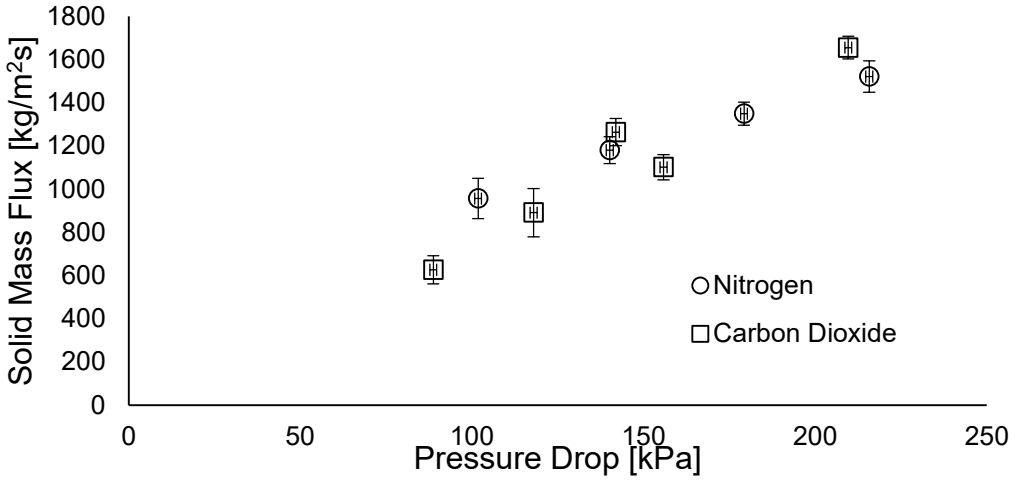

Figure 2-9: Lignite mass flux as pressure drop is varied with different carrier fluids.

2.6 Modelling

A number of models for pneumatic conveying exist to predict the pressure drop profiles for varying conditions. Some of the models are based on first principles, such as a momentum balance, and others use empirical power models to best represent the data.

2.6.1 Sprouse and Schuman (1983) model

The first model considered is by Sprouse and Schuman [14] and consists of a system of equations to be solved simultaneously (Equation 2-2 to Equation 2-7). The equations originate

from two momentum balances; the gas phase momentum balance and solid phase momentum balance.

$$m_s = \frac{m_f(1-\varepsilon)\rho_s}{\varepsilon\rho_f} - \frac{\pi D(1-\varepsilon)^2\rho_s C_{WF} P_R}{\mu b} \quad \text{Equation 2-2}$$

$$m_f = \frac{\pi\varepsilon D^2\rho_f\left(\sqrt{4c_1c_3 + c_2^2} - c_2\right)}{8c_1} \quad \text{Equation 2-3}$$

$$c_1 = \frac{\rho_f}{2C_D^2} \quad \text{Equation 2-4}$$

$$c_2 = \frac{4L\mu\sqrt{b}}{D} \quad \text{Equation 2-5}$$

$$c_3 = \Delta P - \frac{4LC_{WF}(1-\varepsilon)P_R}{D} \quad \text{Equation 2-6}$$

$$b = \frac{150(1-\varepsilon)^2}{\varepsilon^2 d_{31}^2} \quad \text{Equation 2-7}$$

The Sprouse and Schuman model was developed and validated using the volume-diameter mean particle size of the number distribution (corresponding to the arithmetic mean of the volume distribution presented in Figure 2-2), and consists of two parameters that were determined by linear regression: the coefficient of hopper discharge (C_D) and the coefficient of wall friction (C_{WF}). The volume diameter means (d_{31}) for the three fuels are 84 μm for biomass, 40 μm for lignite, and 35 μm for petroleum coke.

The model was compared against the data obtained using fitted coefficients. The fitted parameters C_D and C_{WF} are shown in Table 2-3. The discharge coefficient is the same for all three fuels, which is suitable as the hopper geometry did not change between the different fuels analyzed. The coefficient of wall friction however did change between the three different fuels analyzed. The coefficient was larger for biomass and approximately the same for lignite and

petroleum coke, suggesting an increase in the contribution due to particle friction when the fibrous biomass material is conveyed.

Table 2-3: Parameters from Sprouse and Schuman model determined by a best-fit analysis

	Sprouse and Schuman [14]	**Parameters fit to data**
Coefficient of hopper discharge (C_D)	0.135	0.0878
Coefficient of wall friction (C_{WF})	5.18 x 10^{-6}	1.18 x 10^{-5} (Biomass) 1.71 x 10^{-6} (Lignite) 1.76 x 10^{-6} (Petroleum Coke)

2.6.2 Geldart and Ling (1990) model

Geldart and Ling [15] developed a model for pneumatic conveying that consisted of the summation of different pressure drop terms: particle acceleration, bends, solid head, gas-wall friction, and solid-wall friction. The overall model has the form:

$$\Delta P_{Tot} = \Delta P_{Accel} + \Delta P_{Bends} + \Delta P_{Head} + \Delta P_{GasWall} + \Delta P_{SolidWall} \quad \text{Equation 2-8}$$

$$\Delta P_{Tot} = 2\bar{m}_s U + \frac{n}{2}\bar{m}_s U + \frac{\bar{m}_s H g}{V_p} + \frac{2fL\rho_f U^2}{D} + K\left(\frac{\mu}{\rho_f}\right)^{0.4}\left(\frac{\bar{m}_s}{D}\right)^m \frac{L}{U} \quad \text{Equation 2-9}$$

In Equation 2-9, they assumed the gas-wall friction of a two-phase solid-gas system to be equivalent to that in a single-phase pipe, and f was calculated using the fanning friction factor. They determined the solid-wall friction factor experimentally, and the coefficients K and m were found by correlating the data to two lines at $K = 106$ and $m = 0.83$ for $\frac{\bar{m}_s}{D} < 4.7 \times 10^4$ kg/m^{3}s, and $K = 0.838$ and $m = 1.28$ for $\frac{\bar{m}_s}{D} > 4.7 \times 10^4$ kg/m^{3}s. The data was fit to over 600 data

points of two types of coal conveyed through lines with diameters ranging from 0.62 cm to 1.25 cm. Particle velocity is estimated using the correlation presented in Equation 2-10 [15].

$$V_p = U(1 - 0.0638 d^{0.3} \rho_s^{0.5}) \quad \text{Equation 2-10}$$

2.6.3 Empirical model

The final model compared with the collected data is a purely empirical model. The parameters found in the empirical model include the pressure drop (kPa), the sparge gas flow rate (kg/h), and the transfer gas flow rate (kg/h). The output of the model is the fuel mass flux (kg/m^{2}s), which was shown to not be affected by the fluidizing gas or transfer line diameter in section 2.5. The model parameter coefficients were determined using non-linear regression, and can be found in Equation 2-11 to Equation 2-13 for biomass, lignite, and petroleum coke.

$$\bar{m}_{biomass} = 6.37\,\Delta P + 21.15\,m_{sparge} - 0.21\,\Delta P\,m_{sparge} - 0.266\,\Delta P\,m_{transfer} \quad \text{Equation 2-11}$$

$$\bar{m}_{lignite} = 7.59\,\Delta P + 16.37\,m_{sparge} + 8.32\,m_{transfer} - 0.24\,\Delta P\,m_{transfer} - 15.1\,m_{sparge}m_{transfer} \quad \text{Equation 2-12}$$

$$\bar{m}_{petcoke} = 9.62\,\Delta P + 48.51\,m_{sparge} - 62.28\,m_{transfer} - 0.61\,\Delta P\,m_{sparge} + 2.77\,m_{sparge}m_{transfer} \quad \text{Equation 2-13}$$

The model considers linear and second order interaction effects. Quadratic effects were considered; however, it was found that the inclusion of these parameters did not improve the relative error of the models. Figure 2-10 shows a comparison of the model predictions and experimental values. It can be seen that the models have a good prediction of less than 15% relative error.

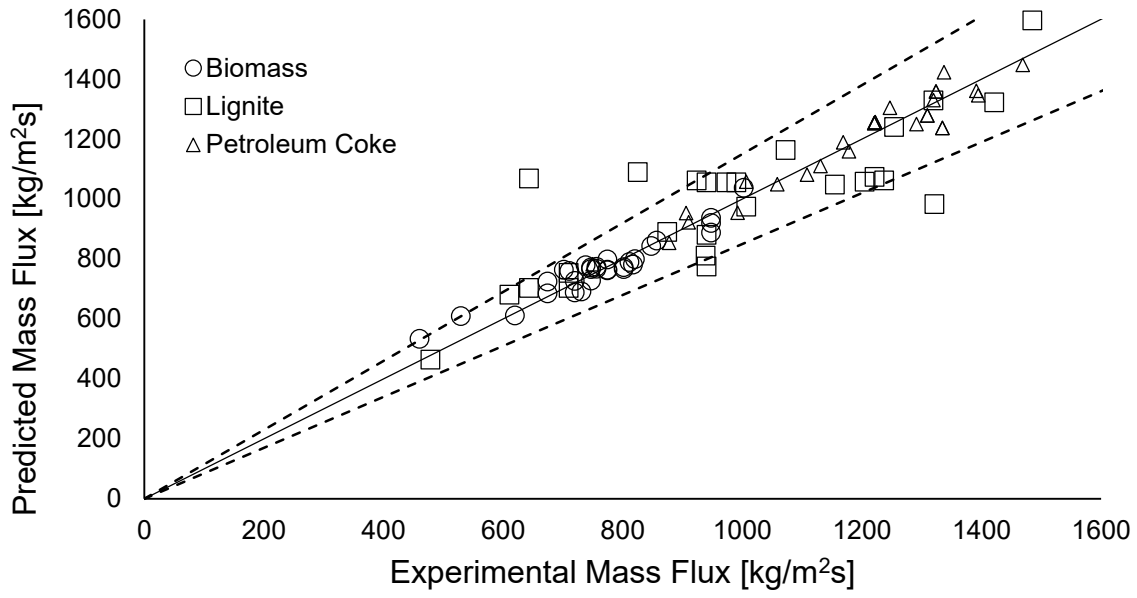

Figure 2-10: Comparison between empirical model prediction and experimental mass flux for biomass, lignite, and petroleum coke. Dashed lines indicate +/- 15%.

2.6.4 Model comparison

The Sprouse and Schuman model is based on fundamental physical properties and behaviour of the fuel and the gas in transit through the transfer line (momentum balance); however, it contains two parameters that are determined by linear regression for a particular fuel and system geometry. The Geldart and Ling model contains no fitted parameters to a particular system geometry; however, it does not have good resolution on particle properties. The empirical model is entirely based on linear regression parameters and is only applicable to the conveying system employed herein; however, it does provide insight as to the relative effect of individual system parameters such as fluidizing gas, sparge gas, and transfer gas. A comparison of the average absolute relative error for three of the models examined with all experimental data collected in this work can be found in Table 2-4.

Table 2-4: Comparison of average absolute relative error for models studied with the three fuels, based on all experimental data obtained.

Method	Biomass	Lignite	Petroleum coke
Sprouse and Schuman	6%	8%	7%
Geldart and Ling	73%	22%	20%
Empirical	4%	11%	4%

In addition to the relative error, the bias for each model can be calculated using Equation 2-14 where a value greater than 1.0 indicates a bias towards overestimation and a value of less than 1.0 indicates a bias towards underestimation. It can be seen that the Geldart and Ling model exhibits a larger relative error than the other models as well as a more significant bias, with the direction depending on the fuel (Table 2-5). The purely empirical model offers a moderately low average absolute relative error with virtually no bias, whereas the Sprouse and Schuman model has a low average absolute relative error, and a marginal bias towards underestimating. The low error and marginal bias indicates that the Sprouse and Schuman model is a good fit.

$$F_m = \exp\left[\frac{1}{k}\sum_{k} ln\left(\frac{estimate}{experimental}\right)\right] \qquad \text{Equation 2-14}$$

Table 2-5: Bias of conveying models for all three fuels, based on all experimental data obtained.

Method	Biomass	Lignite	Petroleum coke
Sprouse and Schuman	0.957	0.975	1.011
Geldart and Ling	1.712	1.117	0.788
Empirical	1.010	1.007	1.001

2.7 Conclusions and Recommendations

After several iterations, a blow vessel configuration was developed that can convey pulverized fuels continuously from a supply hopper to another vessel (such as a reactor) a short distance (14.9 m) away. The vessel consists of a conically shaped hopper with a smooth continuous transition to a 0.77 cm transfer line. A fluidizing ring at the bottom of the vessel supplies carrier fluid to the hopper, which can be used to control the pressure inside the feed vessel, has no significant effect on the average fuel flux. A sparge tube descending through the top of the hopper supplies carrier fluid directly into the bottom cone to prevent material consolidation. The sparge tube also supplies carrier fluid to the sides of the vessel to reduce channeling. Additionally, aeration pads are installed in the conical section of the hopper, oscillating on a 1-minute cycle. This also assists in reducing channeling in the hopper.

The tested fuels consisted of biomass (Geldart class A), lignite (Geldart class C), and petroleum coke (Geldart class C). Although the biomass is classified as type A, suggesting optimal properties for fluidization, it proved the most difficult in conveying, requiring higher gas flow through the transfer line to prevent the material from agglomerating and plugging. Lignite and petroleum coke exhibited similar flow characteristics, suggesting that the particle size and shape has a greater effect than particle density on the flowability of the fuels. System parameters (pressure drop, gas injection point, and gas flow rate) have a reduced effect on biomass flux when compared to their effect on lignite and petroleum coke. Control of the fuel flux can be achieved by manipulating the pressure differential between the supply and destination, the sparge gas, and/or the transfer gas.

The data obtained was compared against two existing pneumatic conveying models, and was found to have a good fit. The Sprouse and Schuman model, which is a model based on

fundamental fluid-particle dynamics, exemplifies the effect of particle wall friction when comparing two fuels with considerably different particle geometries and size distributions.

2.8 Acknowledgements

This work was supported by the Government of Canada's Program of Energy Research and Development, and ecoENERGY Innovation Initiative.

2.9 Nomenclature

β_{ij}	Empirical coefficient [-]
ε	Void fraction [-]
μ	Fluid viscosity [Pa·s]
ρ_f	Fluid density [kg/m^3]
ρ_s	Solid Particle density [kg/m^3]
A_c	Particle cross-section [m^2]
b	Fluid-solids drag constant [m^{-2}]
c_1	First quadratic constant [kg/m^3]
c_2	Second quadratic constant [kg/m^{2}s]
c_3	Third quadratic constant [Pa]
C_D	Hopper Discharge Coefficient [-]
C_{WF}	Coefficient of wall friction [-]
D	Transfer line diameter [m]
d_{31}	Volume-diameter mean of the particle number distribution [m]
d	Particle diameter [m]
d_i	Particle diameter in the size distribution [m]
f	Fanning friction factor of a gas-phase system [-]
g	Gravitational constant [m/s^2]
H	Height difference between inlet and outlet of conveying system [m]
L	Total length of transfer line [m]

m_f	Fluid mass flow [kg/s]
m_s	Solid mass flow [kg/s]
$\bar{m}_s$	Solid mass flux [kg/m^{2}s]
n	Number of bends in the conveying system [-]
ΔP	Pressure drop [Pa]
P_R	Pressure in receiver vessel [Pa]
U	Superficial gas velocity [m/s]
V_p	Particle velocity [m/s]
X_i	Empirical parameter [-]
x_i	Volume fraction of particle size distribution [-]

3. Fuel jet half-angle measurements and correlation for an entrained flow gasifier

FT Kus[ab], MA Duchesne[b], RW Hughes[b], A Macchi[a], P Mehrani[a*]

[a] Department of Chemical and Biological Engineering, University of Ottawa

161 Louis Pasteur Street, Ottawa, Canada, K1N 6N5

[b] Natural Resources Canada, CanmetENERGY

1 Haanel Drive, Ottawa, Canada, K1A 1M1

Manuscript prepared for publication in a journal

3.1 Abstract

Reduced order models (ROMs) are seeing an increasing importance in entrained flow gasification development as a method to reduce computational requirements of reaction modelling. However, due to the simplified nature of ROMs, they require more user inputs in order to properly represent the physics of a reactor. A significant parameter influencing ROM outputs is the jet half-angle of the fuel and oxidant mixture in the gasifier – variations of as little as 1° can change results such as carbon conversion by up to 1% [19]. Thus, it is important to understand the geometry of the jet in the gasifier, and how it is dependent on operating parameters, such as fuel and transport gas flow rates. In this work, the jet half-angle of a non-reactive flow was measured using laser-sheet imaging, for fuel flux ranging 460-880 kg/m^{2}s, and transfer gas flux ranging 43-90 kg/m^{2}s. The jet half-angle was found to be dependent on the solids loading ratio in the jet core. In addition, it correlated well with models developed for liquid systems that are dependent on the ratio of gasifier ambient gas density to jet core density. Jet half-angles ranged from 5.6° to 11.3°, increasing with lower solids loading ratio, for non-reactive cases. The jet half-angle correlation with the gas density ratio was found to hold at high temperature reactive cases as well. Two reactive conditions were calculated by CFD simulation to be 4.9° and 5.7°.

3.2 Introduction

Greenhouse gas emissions over the past 100 years have increased exponentially, resulting in an increased demand for clean alternatives [1]. Integrated gasification combined cycle (IGCC) power plants are considered one of the most attractive technologies for clean power production, due to increased efficiency when compared to conventional power production with carbon capture, and easier gas cleaning due to higher component concentrations in the product gas [4].

The IGCC process includes a gasification unit that converts carbonaceous fuel to a gaseous mixture of CO and H_2 known as synthesis gas, or syngas. The syngas is passed through cleaning units and goes to a gas turbine for power production.

A better understanding of the impact of operational changes during the gasification process has been a research topic for many years. Computational Fluid Dynamics (CFD) is often used to increase understanding in the field due to the high operational costs associated with experimental trials [33,34]. Advantages of CFD models include detailed multi-phase sub-models that can provide insight into the network and kinetics of the reactions. A major drawback associated with CFD modelling is the computation time; a CFD simulation for one condition can take several days and requires high computational power [13].

Reduced order models (ROM) are an alternative to CFD modelling. They require less computational time and power (simulation takes several minutes on a standard work station) while maintaining the integrity of important characteristics of the gasification process such as conversion, temperature profiles, and composition of syngas. The reduced computational time is amenable to study the transient performance of a gasifier [35]. ROMs function on a basis of a reactor network that emulates the geometry and fluid dynamics of the gasifier. As a result of not simulating the complete multi-phase dynamics of the system, to accurately represent the gasifier, a ROM requires more physical input parameters than a CFD model, of which the fuel jet half-angle has a significant impact.

Sahraei *et al*. [19,35] proposed a ROM for the entrained flow gasification unit at CanmetENERGY, in Ottawa, Canada. Their reactor network model consists of three plug-flow reactors (PFR) and two continuous-stirred tank reactors (CSTR). The three PFRs represent two jet expansion zones and one down-stream zone, while the CSTRs represent recirculation zones in

the reactor (see Figure 3-1). The geometry of the reactor models are dictated by the fuel jet half-angle in the reactor vessel, which has been shown to have a significant effect on the carbon conversion and composition of the syngas produced [19,20].

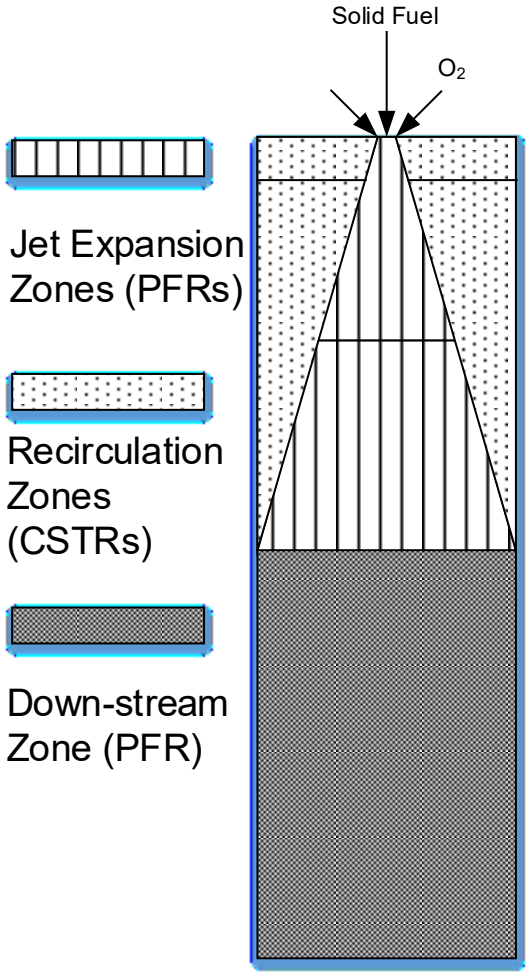

Figure 3-1: Reactor network model developed by Sahraei et al.[19,35]*, representing the different reactor zones within the entrained flow gasification unit at CanmetENERGY.*

Lack of experimental data in the area of fuel jet geometry for gasification systems has resulted in ROMs acquiring jet geometries from CFD simulations [35] or from published values from swirl jets in combustion systems [36]. Consequently, it is of interest to model how the fuel jet half-angle in entrained flow gasifiers varies with changing operating conditions, such as fuel flux and

solid loading ratio, without having to rely on CFD simulations for each condition. In this work, experimental data of jet half-angles for a downdraft entrained flow gasifier at non-reactive conditions are obtained through digital laser sheet imaging and pixel analysis, and used to develop a correlation to predict the jet half-angle and to validate results from CFD simulations.

3.3 Theory

3.3.1 Previous Studies

In the past, studies of two-phase jets have focused largely on the influence of the dispersed phase on the velocity profiles and stability of the jet. Hedman and Smoot [37] determined velocity profiles for two-phase jets of aluminum powder, helium, and air. Modarress [38] determined that solids reduce gas velocity fluctuations. Fleckhaus *et al*. [21] studied the stability and flow structure of a solid-laden jet, and found that the spreading rate of a two-phase jet is smaller than that of a single-phase jet. Numerical studies have also been performed on solid-laden jets with good agreement with available experimental data [39–41]. However, it should be noted that most work regarding solid-laden jets have been done with a relatively low solid loading ratio of $m^* < 1$ (defined as the ratio of mass flow rate of solids (m_s) to the mass flow rate of gas (m_f) as in Equation 3-1). Limited studies performed on dense jets have found that increasing the solid loading ratio reduces velocity fluctuations and the spreading rate [22].

$$m^* = m_s/m_f \qquad \text{Equation 3-1}$$

As mentioned in Section 3.2, it is of interest to determine the half-angle of a gas-solid jet, and determine how it varies with operating parameters such as fuel flow and gas flow injected into the reactor. While modelling of jet half-angles for solid-laden jets is limited, Liu *et al*. [42] found

that dense gas-solid jets behave similarly to liquid jets, implying the jet of dispersed particles flow like a pseudo-homogeneous fluid.

Jet half-angles have been studied in depth for single-phase liquid and gas systems. Ranz [43], and Reitz and Bracco [44] discussed the momentum balance in a liquid jet and outlined the important parameters defining spray dispersion; the square root of fluid jet density ($\sqrt{\rho}$), and fluid jet velocity (u). Wu *et al*. [45] studied the jet half-angle of atomizing jets and found that the influence of aforementioned parameters holds at high pressures, and that the nozzle diameter has no discernable effect on the jet half-angle. Roy *et al*. [46] found that the jet half-angle is proportional to the square root of the ratio of the density of the jet's surroundings (ρ_a) to the density of the jet at the burner exit (ρ_0) (Equation 3-2). They proposed a simple model for the jet half-angle (ϕ) in a liquid jet (Equation 3-3).

$$R = \frac{\rho_a}{\rho_0} = \frac{P_a M_a T_0}{P_0 M_0 T_a} \qquad \text{Equation 3-2}$$

$$\phi = a\, R^{\frac{1}{2}} \qquad \text{Equation 3-3}$$

Chigier and Chervinsky [47] studied gas jet characteristics in a combustion swirl-burner, and found that the jet half-angle is a function of the swirl (S) of the jet (Equation 3-4). They defined the swirl as the ratio of angular momentum to the axial momentum of the jet. Ricou and Spalding [48] studied the mass entrained by a gas injected into a reservoir of stagnant air, and developed a relation (see Equation 3-5). Their model is dependent on the square root of the density ratio ($\sqrt{R}$).

$$\phi = 4.8 + 14S \qquad \text{Equation 3-4}$$

$$\frac{m_e}{m_0} = 0.32\ (R)^{\frac{1}{2}} \frac{x}{d_0} \qquad \text{Equation 3-5}$$

3.3.2 Parametric Analysis

Due to the difficulties of measuring jet angles with reactive conditions, this study was completed with non-reactive conditions (i.e., cold flow). Consequently, the results observed will differ from reactive conditions. The primary physical difference between reactive and non-reactive flow is the temperature. While non-reactive flows will maintain an ambient temperature (about 293 K) throughout the reactor, reactive flows can have ambient temperatures in excess of 2000 K, depending heavily on specific operating conditions (e.g., oxygen concentration, steam injection, etc.).

Beér and Chigier [49] have reported that the jet half-angle of reactive systems is lower than that of non-reactive systems. The density ratio, as shown in Equation 3-2, is dependent on the jet-to-surroundings temperature ratio (T_0/T_a). In non-reactive systems, the jet and surroundings are both at the same temperature, thus the temperature ratio becomes 1. In reactive systems there exists a temperature difference between the jet and the surroundings such that the temperature ratio is less than 1 [13]. Thus the jet half-angle for reactive systems should be lower than the half-angle for non-reactive systems as $\phi \approx \sqrt{T_0/T_a}$.

Another observation discussed by Beér and Chigier [49] is that confinement increases the jet angle. Although jet confinement is not concretely defined by the authors, the underlying principle is that the jet is not permitted to expand freely without influence from a vessel wall. This influence comes in the form of a recirculation zone (Figure 3-1), which increases the effective density of the surrounding gas by increasing the solid loading ratio in area surrounding the jet. For a solid suspension, the effective density, ρ_{eff}, is a function of the solid and fluid volumetric concentration and respective densities (Equation 3-6) [50]. An increase in the

effective density of the surrounding gas results in an increased jet half-angle, as per Equation 3-3 to Equation 3-5. The influence of multiple jets in a gasification system can be anticipated with a similar analysis. The presence of adjacent jets has a similar effect, in that the solids loading and effective density of the surroundings of the first jet increases. The increase of the jet's surrounding density results in a higher jet half-angle.

$$\rho_{eff} = \varepsilon\rho_f + (1-\varepsilon)\rho_s \qquad \text{Equation 3-6}$$

3.4 Experimental Setup

The pressurized gasification pilot plant at CanmetENERGY (Ottawa, ON, Canada), discussed in Chapter 2 [51], was used to conduct a jet geometry analysis on high pressure cold flow pneumatic conveying, using the burner design shown in Figure 3-2. The burner consists of a center tube (ID = 6.2 mm) that conveys a mixture of fuel and carrier fluid into the reactor, and a series of eight impinging jets (ID = 4.4 mm) to mix an impinging gas into the fuel jet. Additionally, a sleeve introduces steam into the reactor. The fuel used in the study is petroleum coke (average particle size d_p = 10 μm, particle density ρ_s = 1176 kg/m^3) [51].

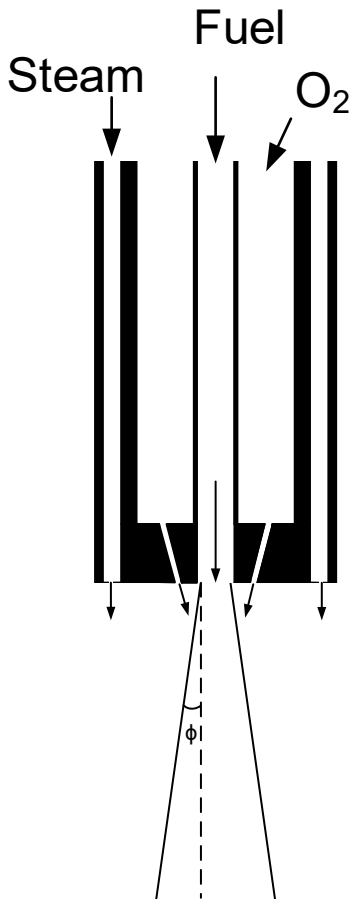

Figure 3-2: CanmetENERGY downdraft entrained flow gasifier burner

The jet geometry imaging was done using a Phantom v9.1 camera with a maximum image capture frequency of 1000 Hz and a resolution of 1,632 x 1,200 pixels, and a Nano L laser by Litron Lasers producing a laser sheet with a thickness of 5 mm on which the images were captured. The laser has a maximum frequency of 15 Hz. A frequency of 10 Hz was used in this work. The laser sheet was in line with the centre of the jet injected by the burner – it should be noted that an analysis was briefly done to study the importance of centering the laser, and found that an offset of as little as 7 mm resulted in skewed jet angles recorded by the imaging software. The camera and laser setup is depicted in Figure 3-3, and discussed in more detail in Daviault *et*

al. [52]. The imaging process was done over a period of 30 seconds for each test, generating 300 images per test.

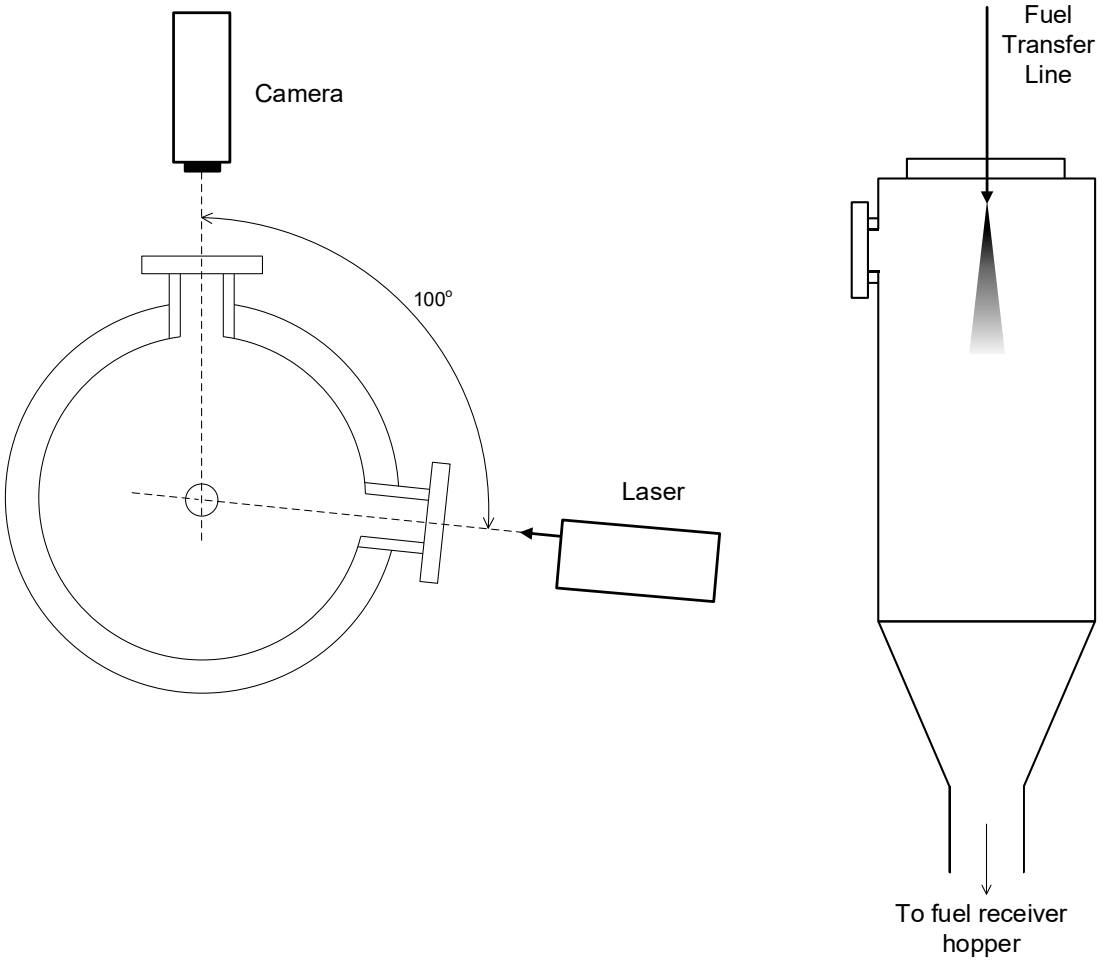

Figure 3-3: Schematic of CanmetENERGY's pneumatic transport system's visualization spool; cross-sectional top view (left) and side view (right).

A mean image for each test was generated using Dantec Dynamics's DynamicStudio software, and the mean jet angle was measured using the software's built-in spray characterization tool, which measures jet angle using a pixel detection method. Thus the boundary of the jet is defined by the particle density in the jet – the edge being the point at which the density is too low for the

equipment to detect particles. The measurements were taken at an axial distance of 84 mm from the burner orifice.

Three tests were performed at each condition to ensure the true mean jet angle was found. The error bars reported in the figures herein represent the standard deviation of the jet angle found for the three tests at each condition. Image masking ensured that the software did not account for recirculating particles as individual jets. Figure 3-4 is an example of the image mean taken for a test condition. Due to the density of solids in the jet, the laser sheet was unable to penetrate completely through the jet. Thus, only an image of one side of the jet was obtainable. The jet is assumed to be axisymmetrical. The tests were performed at room temperature, with a pressure in the reaction chamber of 16 bar. A series of tests were performed at a reaction chamber pressure of 8 bar. The tests were performed using nitrogen as the fuel carrier fluid. Nitrogen was also used as the impinging gas, which would normally be the oxygen injection point for the gasification reaction. This was done due to the low cost of nitrogen, as well as the similar physical properties of the two gases (diatomic molecules, similar gas densities and viscosities). Finally, nitrogen was also used in place of steam, in order to preserve the fuel's dry state to be reused in the conveying system.

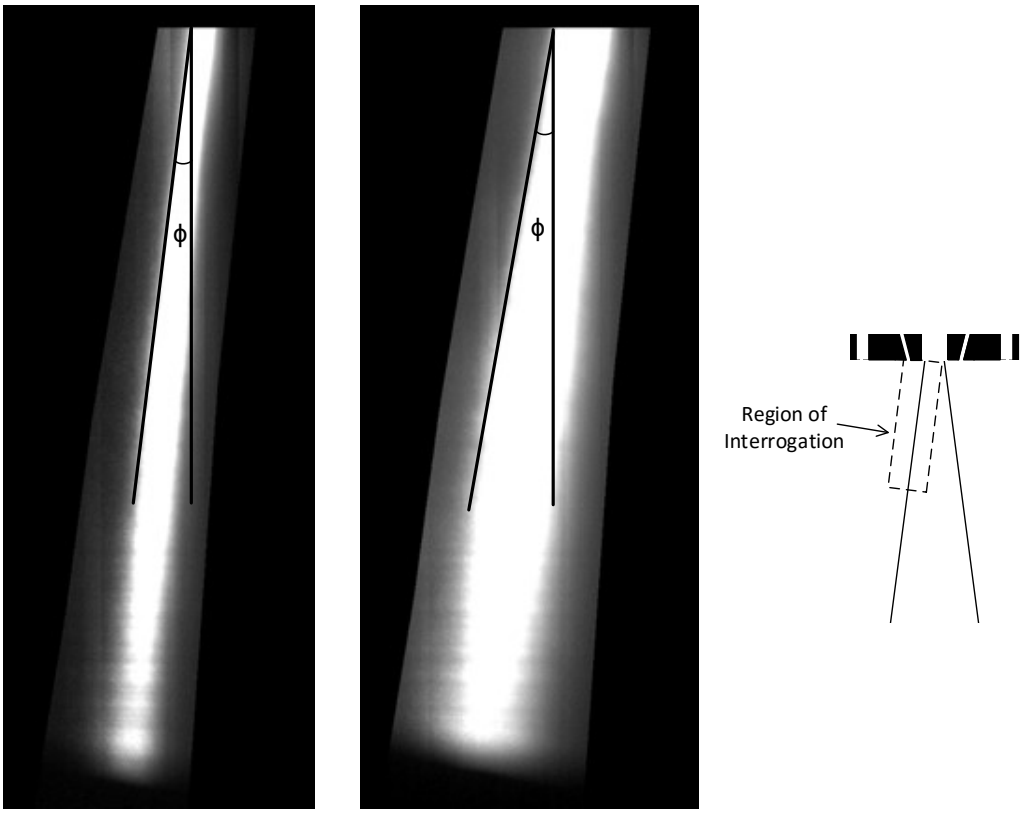

Figure 3-4: Resulting image mean generated from a set of data encompassing 300 images taken at a frequency of 10 Hz (without impinging gas on the left, with impinging gas in the middle, schematic indicating the region of interrogation on the right).

The conditions analyzed were chosen to complement work done on the pneumatic conveying of the pulverized fuel [51], as well as to emulate hot flow conditions of CanmetENERGY's pilot-scale gasifier. Fuel flux ranged 460-880 kg/m^{2}s, with gas flux ranging 43-90 kg/m^{2}s. Jet geometries were analyzed with and without the influence of nitrogen flowing through the steam sleeve and impinging gas from the oxygen injection holes.

3.5 Results and Discussion

3.5.1 Experimental Results

Gas impingement was initially omitted to observe the influence of flow conditions on the jet angle without external interaction. The solids loading ratio (m^*) in the fuel conveying line was observed to have a direct impact on the jet half-angle: as the loading ratio is increased, the jet half-angle decreases (Figure 3-5). In order to ensure this is not a direct result of varying individual flow rates, two test conditions with similar loading ratios but with differing fuel and gas flow rates are compared (Table 3-1): two conditions with a difference in loading ratio of less than 1%, but with a difference in fuel flow of 12% and a difference in gas flow of 11% have the same jet half-angle.

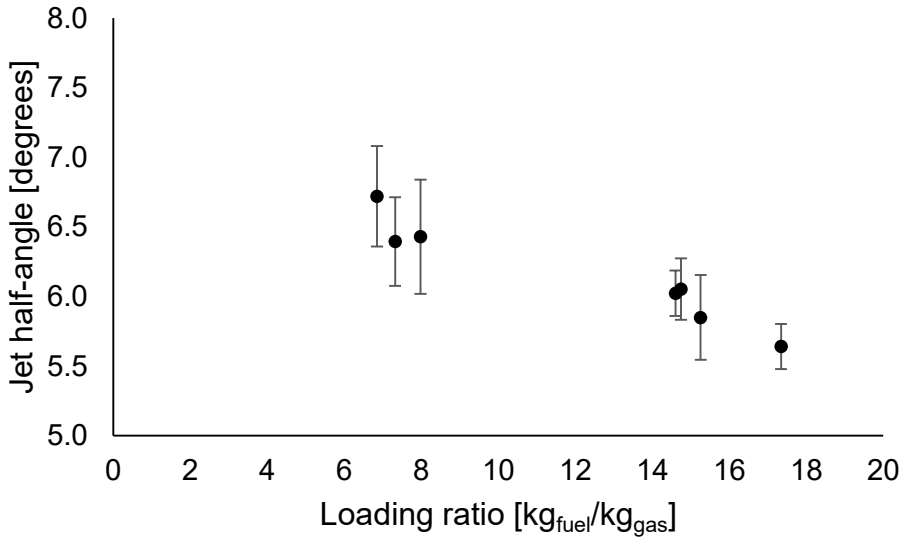

Figure 3-5: Influence of the solids loading ratio on the jet half-angle for a pressure of 1600 kPa

Table 3-1: Influence of fuel and gas flow rates at similar loading ratio on jet half-angle

Solid fuel flow [kg/h]	Gas flow [kg/h]	Loading ratio [kg_{fuel}/kg_{gas}]	Jet half-angle [degrees]
84	5.7	14.7	6.1 ± 0.1
74	5.1	14.6	6.0 ± 0.1

Introduction of the impinging gas increased the jet half-angle by a significant margin, mostly due to the quantity of nitrogen injected into the jet. A comparison of the results obtained with and without gas impingement can be made, assuming that an effective loading ratio (m'^{*}) encompasses the fuel conveying gas and impinging gas (Equation 3-7). For the cases studied here, the impinging gas flow rate was approximately four times larger than the conveying gas flow rate (40 kg/h compared to 8-10 kg/h). As shown in Figure 3-6, the relation observed in Figure 3-5 between loading ratio and jet half-angle holds true when introducing impinging gas.

$$m'^{*} = \frac{m_s}{m_{f,conveyed} + m_{f,impinged}} \qquad \text{Equation 3-7}$$

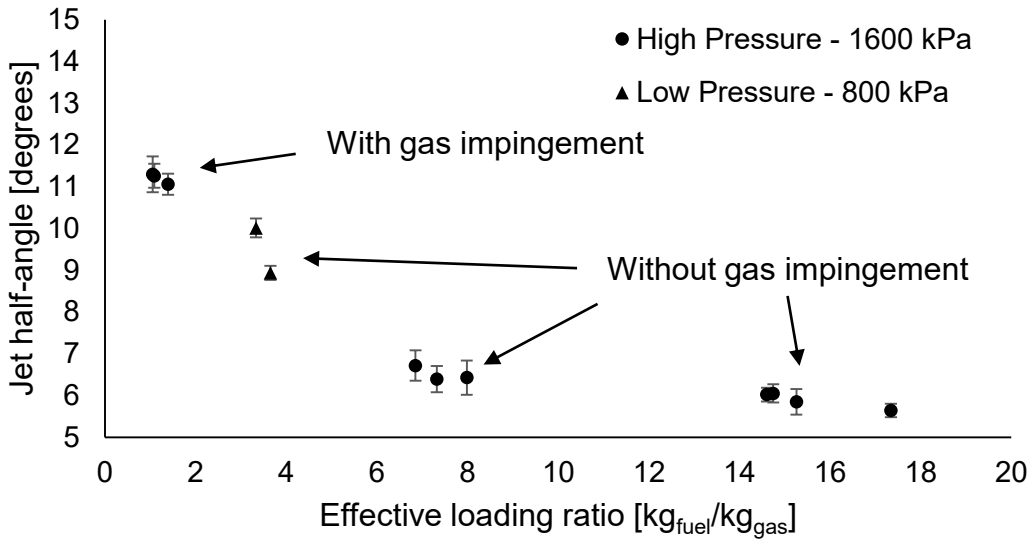

Figure 3-6: Influence of the effective solids loading ratio on the jet half-angle.

The "steam injection" was also varied between two values – 0 and 10 kg/h N_2. These values were selected based on hot flow conditions used with CanmetENERGY's pilot scale gasifier, which was operated with a steam flow rate of up to 20 kg/h H_2O. A value of 10 kg/h N_2 was selected to remain within the range of momentum of the steam entering the reactor (10 kg/h N_2 having the momentum equivalent of 8 kg/h H_2O). The flow of gas entering via the steam injection sleeve did not impact the jet half-angle during cold flow testing. However, during hot flow, steam reduces the reactor temperature which should influence the jet half-angle as discussed in Section 3.3.2 and reported in Beér and Chigier [49].

3.5.2 Model Fitting

The relationship put forth by Roy *et al.* [46] (Equation 3-3) shows that the jet half-angle is inversely proportional to the jet core density. This dependence is analogous to the solid loading ratio, m^*; as the solid loading ratio increases, the effective density of the suspension also increases. Thus, the jet half-angle should be inversely proportional to the solid loading ratio. This

relationship is exemplified in Figure 3-6, where the jet half-angle increases as the solid loading ratio decreases.

Using least squares regression to determine the appropriate constant for the system at hand yields Equation 3-8. This correlation is found using the experimental data acquired during the cold flow experiments. The coefficient of determination of the resulting model is 0.84.

$$\phi = 17.3\, R^{\frac{1}{2}} \qquad \text{Equation 3-8}$$

Two simulations were completed by CanmetENERGY's CFD group with similar conditions as the experiments, in order to determine the jet half-angle for reactive flow. The average temperature in the reactor was calculated to be around 1150 K, while the jet core remains at ambient temperature (298 K). The resulting jet half-angles of the hot flow conditions are 4.9º and 5.7º. Table 3-2 highlights the relevant parameters when modelling the jet half-angle for the two hot flow conditions, and compares them with two of the cold flow experiments carried out at similar conditions. The accuracy of Equation 3-8 for reactive systems demonstrates the strong dependence the jet half-angle has on the density ratio of the jet core and surroundings, fortifying the notion that the momentum of the jet and surroundings is the dominating factor in determining the jet geometry. Figure 3-7 shows the accuracy of the prediction model, Equation 3-8.

It should be noted that the CFD calculated angles from the two hot-flow conditions displayed in Table 3-2 contradict the trend discussed in the previous section (i.e. the half-angle is lower for the condition at a lower solid loading ratio). The hot-flow conditions are not uniformly at the same temperature – rather, the temperature indicated is an estimated average temperature along the length of the jet (see Figure 3-8 for the CFD temperature profile). Consequently, the mean

temperature of the condition at lower loading ratio could be interpreted as higher than that of the higher loading ratio condition, which would justify the lower half-angle calculated by the CFD model. However, the purpose of including these conditions is to demonstrate the overall effect of temperature: that increasing temperature in the reactor (i.e. reactive conditions) result in a lower half-angle that is adequately represented by the change of the jet's surrounding gas density.

Table 3-2: Comparison of jet half-angle modelling for reactive and non-reactive systems

Fuel Flow [kg/h]	Gas Flow (including impinging gas) [kg/h]	Effective Loading Ratio	Temp [K]	Calculated Half-Angle [deg]	Experimental* or CFD Generated Half-Angle [deg]
53	48.7	1.09	298	12.1	11.3*
50	47.7	1.03	298	12.2	11.1*
41	45.4	0.90	1200	6.3	4.9
60	51.1	1.17	1200	5.9	5.7

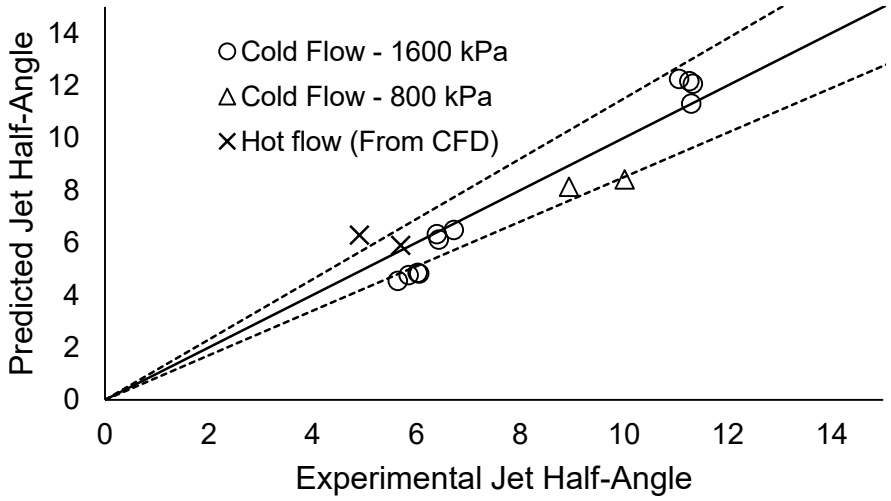

Figure 3-7: Jet half-angle model prediction error; dashed indicate +/- 15%. R^2 = 0.84.

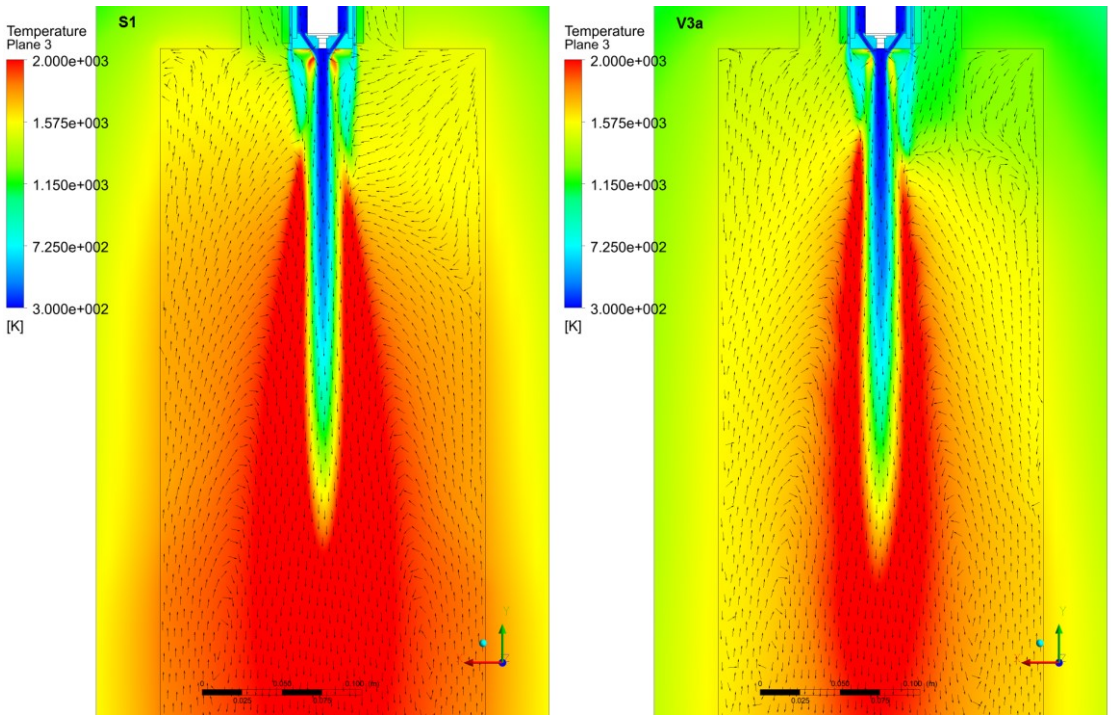

Figure 3-8: CFD generated temperature profile of petroleum coke gasification in an entrained flow reactor, corresponding to the conditions in Table 3-2 (S1 = 41 kg/h; V3a = 60 kg/h).

3.6 Conclusion

Gasification jet half-angles were measured using the burner design described in Section 3.4, consisting of a straight tube injecting a solid fuel suspension, a series of impinging jets for oxygen injection, and a sleeve for steam injection. The jet half-angles were shown to decrease as the effective solid loading ratio was increased in the jet core, which corresponds to an increase of the effective suspension density, and a decrease of the density ratio R. This observation is consistent with correlations proposed in previous works suggesting the jet half-angle is dependent on the ratio of momentum between the jet surroundings and the jet core, and a model was proposed correlating the jet half-angle to the ratio of densities between the jet surroundings and core. The resulting model was verified by CFD simulation of hot flow conditions. The

increase in temperature influences the gas density in the reactor surroundings such that the jet half-angle is adequately modelled with Equation 3-8. Future work on studying the variability of the jet angle at different gasifier operating conditions (pressure, solid loading ratio) would be beneficial.

3.7 Acknowledgements

This work was supported by the Government of Canada's Program of Energy Research and Development, and ecoENERGY Innovation Initiative. The authors would like to acknowledge Richard Lacelle, Scott Champagne, Dr. Dennis Lu, Robert Yandon, David McCalden, Alex McCready, Jeffrey Slater and Christopher Mallon for their aid with the experimental work.

3.8 Nomenclature

a	Constant [-]
d	Diameter [m]
M	Molar Mass [g/mol]
m	Mass Flow Rate [kg/h]
m^*	Fuel Loading Ratio [kg_{fuel}/kg_{gas}]
m'^*	Effective Fuel Loading Ratio [kg_{fuel}/kg_{gas}]
P	Pressure [kPa]
R	Density Ratio [ρ_a/ρ_o]
S	Swirl [-]
T	Temperature [K]
ε	Suspension Void Fraction [-]
ρ	Density [kg/m^3]
ϕ	Jet Half Angle [degrees]

Subscripts

a	Ambient
e	Entrained
eff	Effective (in reference to a solid-gas suspension)
f	Fluid
o	Jet core, or jet orifice
s	Particle, or solid

4. Frequency analysis of a pneumatic conveying system

4.1 Introduction

The gasification process consists of the thermochemical conversion of a carbonaceous fuel to a gaseous mixture of hydrogen and carbon monoxide known as syngas via Reaction 4-1. The reaction requires a specific fuel-to-oxygen ratio to maintain a high yield of syngas; an increase in oxygen will result in combustion taking place in the reactor (Reaction 4-2) [23].

$$C_nH_m + \frac{n}{2}O_2 \rightarrow n\,CO + \frac{m}{2}\,H_2 \qquad \text{Reaction 4-1}$$

$$C_nH_m + \left(n + \frac{m}{4}\right)O_2 \rightarrow n\,CO_2 + \frac{m}{2}\,H_2O \qquad \text{Reaction 4-2}$$

In order to maintain a constant fuel-to-oxygen ratio, the fuel feed rate to the reactor must be reliable, with minimal variability. Fluctuations in fuel flow directly influence the gasifier performance, as the reaction shifts between gasification and combustion, which reduces the energy value of the product gas by diluting it with CO_2 and H_2O. Experiments performed in Chapter 2 of this thesis have shown significant variation of fuel flow over time. Experiments performed in Sprouse *et al.* [53] show the same variability.

Modelling the influence of fuel flow variability on reactor performance requires transient modelling of the gasification process. As mentioned in Sections 1.1 and 3.2, gasification modelling is quite complex, and is typically done in the form of computation fluid dynamics (CFD). The large computational requirements of CFD analysis make transient modelling unattractive, as it takes up to several days for a steady-state condition to converge. Reduced order models (ROMs) offer a low-computational alternative to CFD simulations [12], are a plausible tool for modelling the transient behaviour of gasifiers as they can be used to calculate

time-dependent outlet conditions based on a time-dependent input function. In Chapter 2 [51], the Sprouse and Schuman [14] model was shown to adequately predict the mean flow rate of pulverized solid fuels as a function of the pressure drop, gas flow rates, and conveying line configuration. This model can be used to predict the transient behaviour of the fuel flow as these conditions are varied. Figure 4-1 shows that the predicted mass flow still does not accurately represent the variation observed in the experiments. A mathematical model representing the variation in the fuel flow over time needs to be determined, and used in conjunction with the Sprouse and Schuman [14] model in a ROM to determine the impact of fuel fluctuations on gasifier performance.

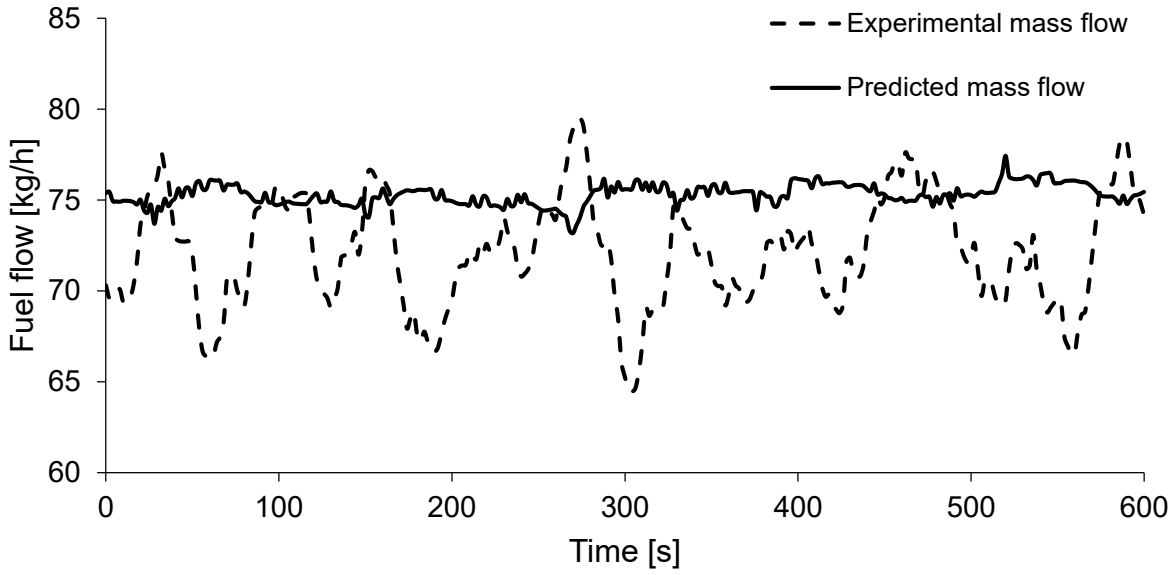

Figure 4-1: Comparison of experimental flow rate and modeled flow rate (Sprouse and Schuman [14]*) of pulverized petroleum coke from a hopper in a pneumatic conveying system with sparge and fluidizing gas flow rates of 4 kg/h, a transfer gas flow rate of 1 kg/h, and a pressure drop of 155 kPa.*

4.2 Frequency Analysis

A reliable characterization method for the fuel flow variability must be established before a model can be developed. A powerful method for quantifying fluctuations in a time-series data set is to perform a frequency analysis. Frequency analysis methods have been employed in the study of fluidized beds as a method for characterizing the different flow regimes [54–57] by analyzing pressure fluctuations. A frequency analysis consists of converting the data from the time-domain into the frequency-domain using Equation 4-3 [58–60]. The Fast-Fourier transform is often used to generate the frequency-domain function.

$$F(\omega) = \sum_{t=-\infty}^{\infty} f(t)\exp[-i\omega t] \qquad \text{Equation 4-3}$$

The method produces a series of frequencies (ω) with a corresponding amplitude (A) and phase (ϕ). The maximum frequency that can be characterized by this analysis is the Nyquist frequency, which is half of the sampling rate of the time-series data set. The number of frequencies returned by a Fast-Fourier transform is dependent the number of points in the data set (half the number of data points plus one). For instance, a ten-minute sampling period with a sampling rate of 2 s (0.5 Hz), results in 300 sample points. The maximum frequency characterized is 0.25 Hz, with 151 frequencies observed (0 Hz, 0.25/150 Hz, 0.50/150 Hz, 0.75/150 Hz, etc.). The time-series function $f(t)$ can be reconstructed from the Fourier-series $F(\omega, A, \phi)$ using Equation 4-4, for all frequencies ($\omega_0, \ldots, \omega_n$).

$$f(t) = \sum_{i=0}^{\mathrm{n}} A_i[\sin(2\pi\omega_i - \phi_i) + \cos(2\pi\omega_i - \phi_i)] \qquad \text{Equation 4-4}$$

4.3 Experimental Setup

4.3.1 Equipment and Software

The equipment used in these experiments are described in Section 2.4 [51]. The fuel flow rates were measured using load cells calculations. The change in mass of the feed supply hopper was measured over a 30 second period, and a moving average function was used to calculate the flow of material from the hopper. The load cells have a maximum refresh rate of 366 Hz, with a maximum update rate to the control interface of 20 Hz. The measurements were recorded at a rate of 0.5 Hz (2 s intervals). The frequency analysis was performed using Origin® 2015. The software has a built-in Fast-Fourier transform function that allows for rapid calculation of the frequency domain based on a time domain input. The number of peaks that are returned (151 peaks for a 10-minute sample) can result in a cumbersome analysis, and an inconvenient mathematical model composed of several sinusoidal functions. Therefore, it is if interest to determine the significant peaks that can adequately represent the variability of the fuel flow. Origin® 2015 has a built-in "Peak Analyzer" tool that returns the highest peak in a defined range of data points.

4.3.2 Method

The frequency analysis was performed first on three no-flow conditions, in order to determine which peaks can be attributed to measurement error. One of the no-flow conditions was broken down into segments of 3-min, 5-min, 10-min, and 13-min in order to determine the minimum amount of data required to achieve a reliable resolution on the frequency domain.

The time-series data set comprised of the error of the predicted flow rate (by the Sprouse and Schuman [14] model) and the experimental flow rate was analyzed in the frequency-domain. The

peak analyzer tool was used to determine the significant peaks within a ten data point range. The peaks were then compared with the list of peaks attributed to error. Peaks that can be associated to error are rejected, while the remaining peaks can be used to study the behaviour of the fuel flow, and generate a mathematical model.

4.4 Results and Discussion

4.4.1 Sample size

A no-flow condition was used to establish an appropriate time-series sample size. Figure 4-2 shows the resulting frequency-domain for four different test periods (13 minutes, 10 minutes, 5 minutes, and 3 minutes), and Figure 4-3 shows the significant peaks for the different time intervals. Longer testing periods result in a higher resolution in the frequency-domain. The 3-minute period observed significantly less precision than the others, as the peak analyzer tool was unable to recognize most of the peaks. Increasing the test period above the 10-minute mark did not appear to add significant precision, as the 10-minute and 13-minute periods show similar results.

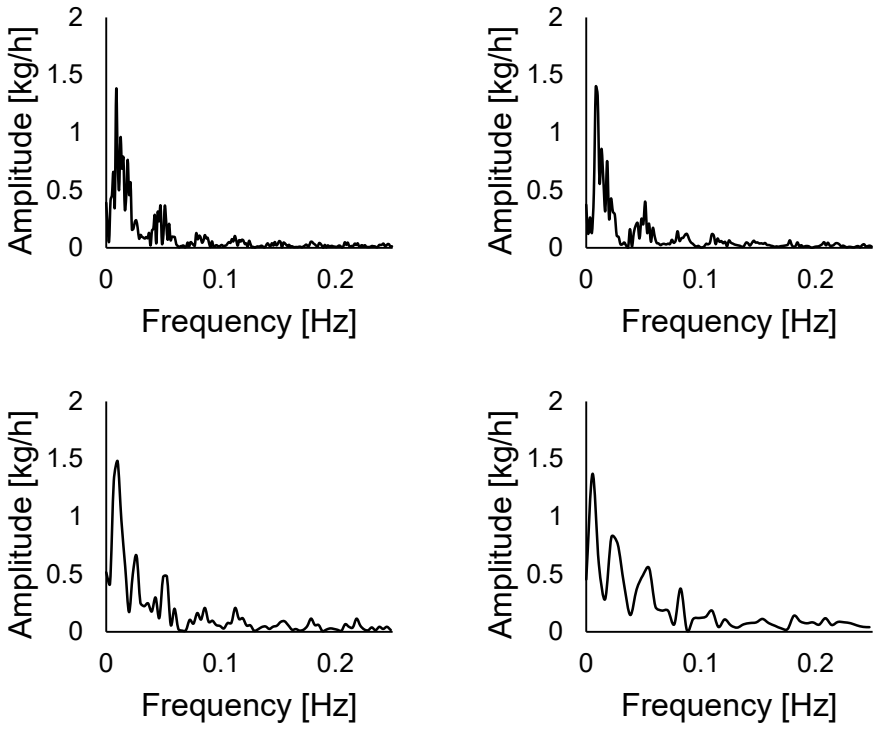

Figure 4-2: Frequency-domain results for a no-flow condition, analyzed over a 13-minute period (top-left), a 10-minute period (top-right), a 5-minute period (bottom-left), and a 3-minute period (bottom-right).

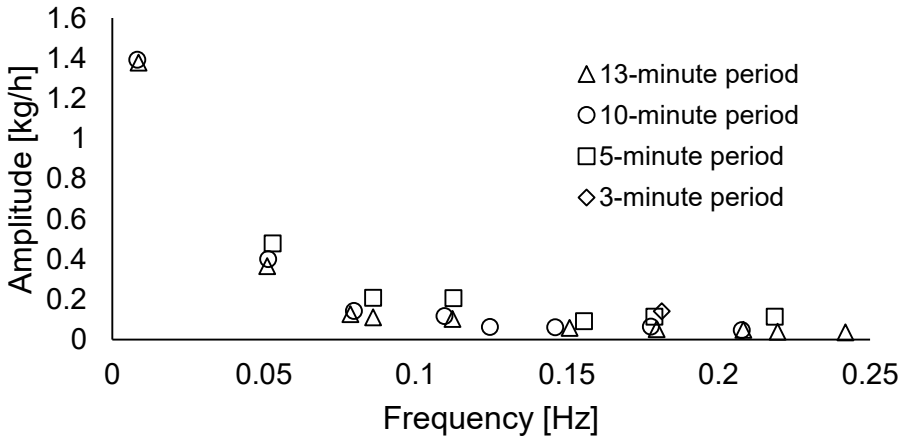

Figure 4-3: Frequency-domain significant peaks determined by Origin® Peak Analyzer for a no-flow condition at different test periods.

4.4.2 Determining error

In order to determine the error associated to the equipment, three no-flow conditions were analyzed in the frequency-domain. The significant peaks observed at these no-flow conditions are shown in Figure 4-4. Further analysis can be compared to Figure 4-4 to determine if the peaks observed can be attributed to error, or if they are a true representation of the fuel flow variability.

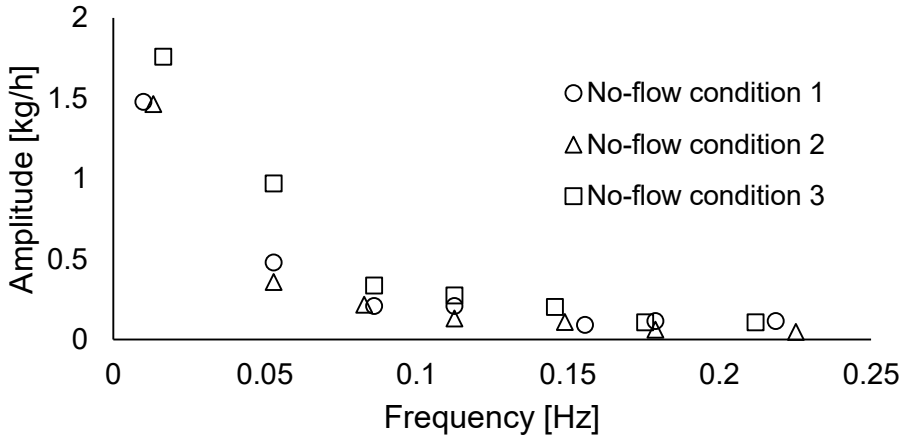

Figure 4-4: Frequency-domain significant peaks from three no-flow conditions over a 10-minute analysis period.

The highest peak in Figure 4-4 is observed at a frequency of 0.016 Hz, which corresponds to a cyclic flow fluctuation every 60 s. Note from section 2.4 that the conveying system uses aeration pads on a 60 s cycle to prevent material consolidation and channelling within the hopper. The amplitude observed at this frequency (1.5-1.8 kg/h) corresponds to the gas surged into the feed vessel over a 10 s period, every 60 s (3.15 kg/h gas, corresponding to an amplitude of 1.58 kg/h).

4.4.3 Frequency analysis: base case

Petroleum coke conveyed through a 0.46 cm ID stainless steel tube, with a pressure difference between the feed hopper and receiver hopper of 155 kPa, a fluidizing gas flow rate of 4 kg/h, a sparge gas flow rate of 4 kg/h, and a transfer gas flow rate of 1 kg/h was chosen as the base case. A Fast-Fourier transform was performed on a 10-minute period of the base case, and the significant peaks were calculated from the resulting frequency-domain. Figure 4-5 shows the significant peaks, and compares them to a no-flow condition that was previously used to determine measurement error.

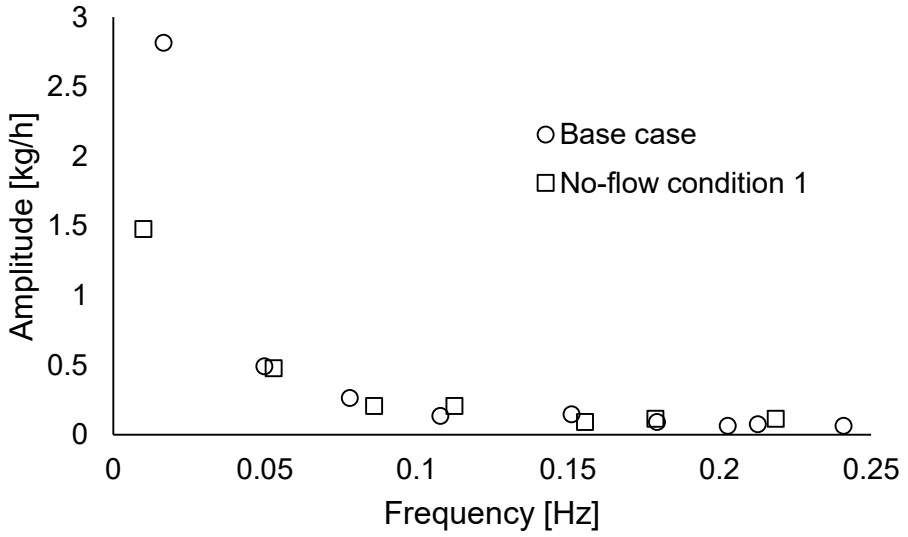

Figure 4-5: Frequency-domain significant peaks of the base case (petroleum coke, 155 kPa pressure drop, fluidizing and sparge gases at 4 kg/h, transfer gas at 1 kg/h) and one of the no-flow conditions.

Most of the peaks observed can be attributed to measurement error. However, peaks for the base case at a frequency of 0.016 Hz are significantly greater than the peaks observed in the no-flow cases (almost twice as high, with a value of 2.8 kg/h versus the no-flow value of 1.5 kg/h). The presence of significant peaks at this frequency suggest that the aeration pads are assisting in fuel

discharge from the feed hopper. Peaks observed at higher frequencies correspond to error previously established (Figure 4-4), and can not be used to describe the variability of fuel transport.

4.4.4 Effect of pressure drop

The pressure drop between the feed hopper and receiver hopper was varied around the base case, and the effect on the significant peaks in the frequency-domain can be seen in Figure 4-6. As the pressure drop is increased, the amplitude of the significant peaks increases, observed in Figure 4-7. This is consistent with the pneumatic conveying trend of increased fuel flow with increasing pressure. At a frequency of 0.016 Hz – when the aeration pads pulsate – fuel discharge from the feed hopper is increased by an amount proportional to the pressure drop across the transfer line.

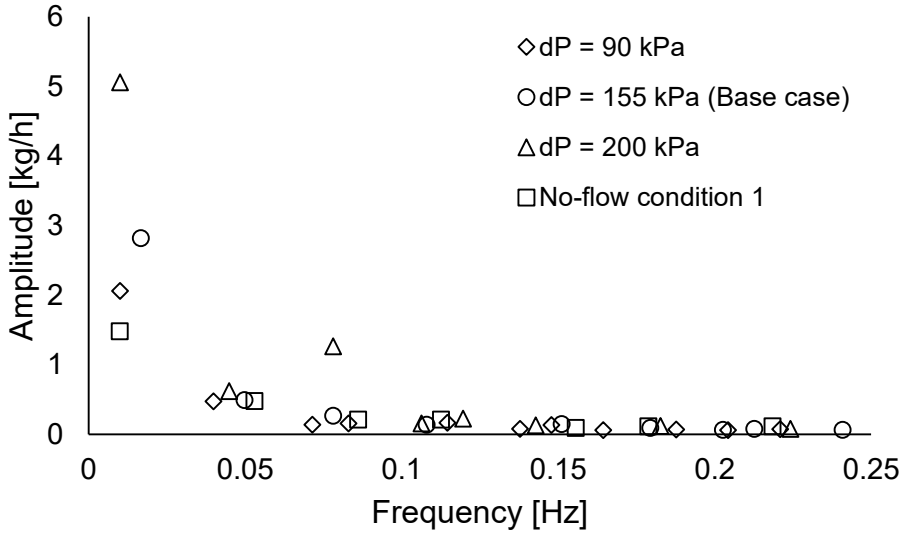

Figure 4-6: Frequency-domain significant peaks of conditions with differing pressure drops between the feed hopper and receiver hopper (petroleum coke, fluidizing and sparge gases at 4 kg/h, transfer gas at 1 kg/h) and of one of the no-flow conditions. Total gas flow rate in the transfer line is 4.3, 4.6, and 5.2 kg/h for 90, 155, and 200 kPa respectively.

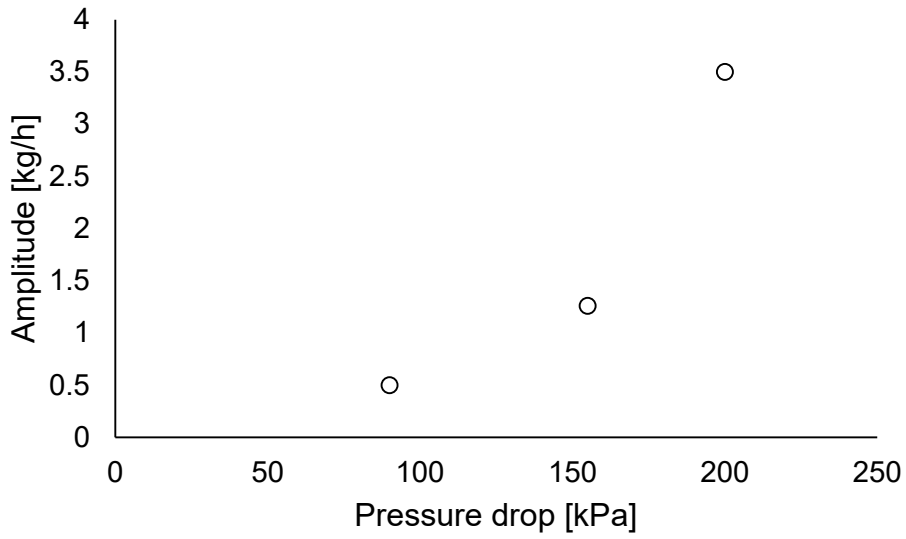

Figure 4-7: Amplitudes of significant peak (at a frequency of 0.016 Hz), corrected for the error associated with the no-flow conditions.

4.4.5 Effect of gas flow rate

The influence of the gas flow rate in the transfer line on the mean flow rate of pulverized fuels in a pneumatic transport system is discussed in Chapter 2: increasing the gas flow rate in the transfer line reduces the fuel flow rate, due to the dilution of solid fuel with gas. Figure 4-8 shows the significant peaks of the frequency-domain for different gas flows. Figure 4-9 shows that the amplitude of the significant peak observed decreases as the gas flow rate increases, which is consistent with observations regarding the fuel flow characteristics. The two high gas flow rate points on Figure 4-9 are below the abscissa, indicating that they are within the range of the error measured by the no-flow conditions, which can be seen in Figure 4-8.

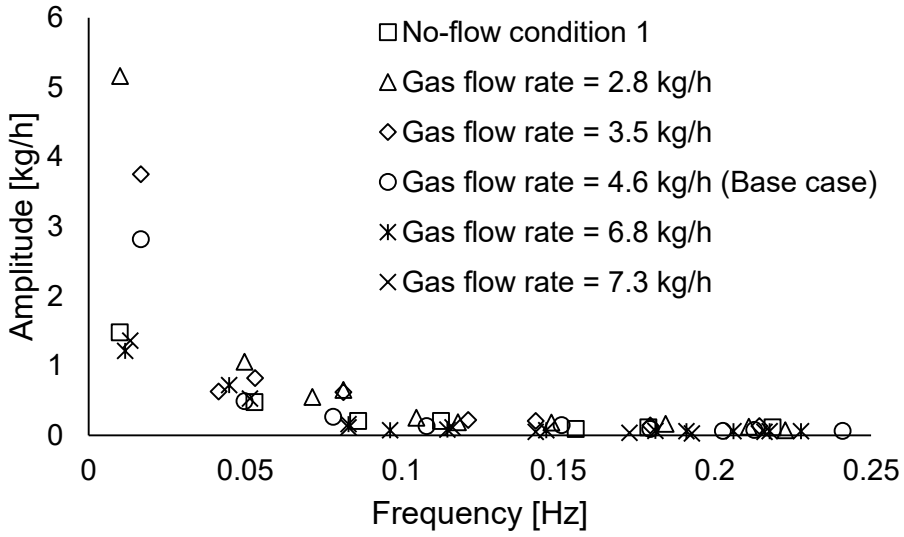

Figure 4-8: Frequency-domain significant peaks of conditions with differing total gas flow rates in the transfer line, for a pressure drop of 155 kPa, and one of the no-flow conditions.

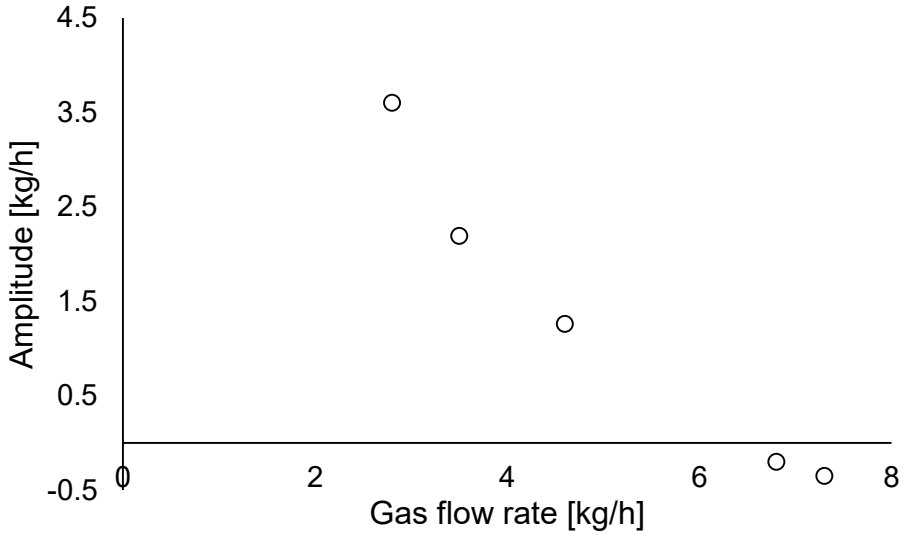

Figure 4-9: Amplitudes of significant peak (at a frequency of 0.016 Hz), corrected for the error associated with the no-flow conditions.

4.4.6 Modelling

In order to understand the influence of the fuel flow variability on the gasification process, ROMs can use the time-domain function of the frequency analysis to estimate performance parameters, such as carbon conversion and syngas yield. The time-domain function is dependent on the amplitude and phase for any given frequency. Due to the lack of multiple significant peaks, the phase associated with the time-domain function does not affect the overall estimated variability, and the equation is simplified (Equation 4-5). The coefficient A_i, corresponding to the amplitude at frequency ω_i = 0.016 Hz, for each of the conditions studied can be found in Table 4-1.

$$f(t) = \sum_{i=0}^{n} A_i[\sin(2\pi\omega_i) + \cos(2\pi\omega_i)] \qquad \text{Equation 4-5}$$

Table 4-1: Amplitudes of significant peaks at a frequency of 0.016 Hz for the different conditions studied in this work.

Pressure drop [kPa]	Gas flow rate [kg/h]	Amplitude, A_i [kg/h]
90	4.3	0.5
155	4.6	1.26
200	5.2	3.5
155	7.3	0
155	6.8	0
165	2.8	3.6
165	3.5	2.19

The equation can be used in conjunction with the Sprouse and Schuman model discussed in Chapter 2. Figure 4-10 shows the resulting model with the frequency analysis model incorporated as a correction factor, and compares it to the experimental results. The model

provides a more representative prediction of the fuel flow rate over a 10-minute period, and can be used in conjunction with a ROM to determine the impact of the variability of the fuel flow on the performance of an entrained flow gasification system.

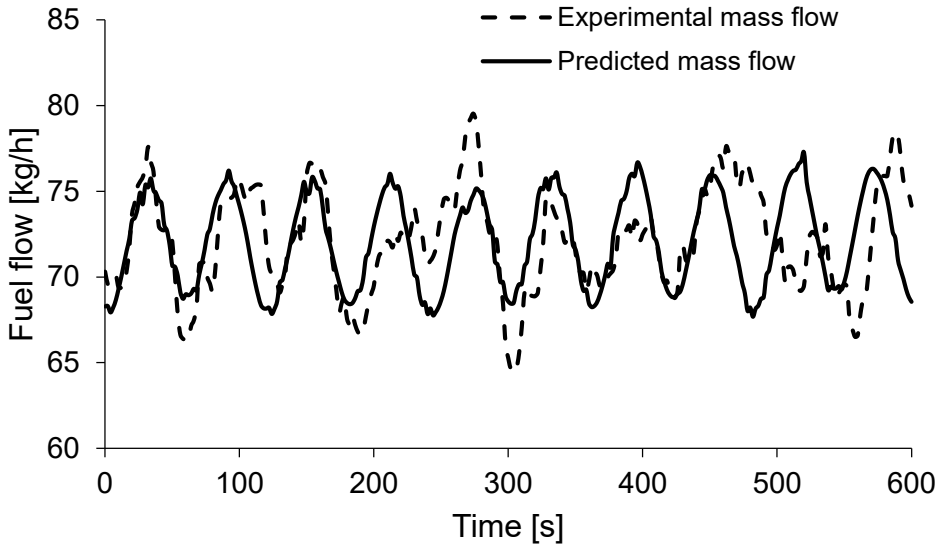

Figure 4-10: Comparison of experimental flow rate and modeled flow rate (Sprouse and Schuman [14]*) with the frequency analysis correction factor (Equation 4-5) of pulverized petroleum coke from a hopper in a pneumatic conveying system with sparge and fluidizing gas flow rates of 4 kg/h, a transfer gas flow rate of 1 kg/h, and a pressure drop of 155 kPa.*

4.5 Conclusion

The fuel flow variability in a pneumatic transport system was quantified using a frequency analysis, which consisted of performing a Fast-Fourier analysis on a time-domain data set using the software Origin® 2015. The measurement error was first established by performing the analysis on a set of no-flow conditions, which were then compared to the results from other conditions. It was found that the only peak that is not associated with measurement error is the peak found at a frequency of 0.016 Hz. This frequency coincides with the pulsating frequency of the aeration pads in the system, suggesting that these pads assist discharging the fuel from the

feed hopper. The influence of pressure drop and gas flow rate in the transfer line were studied, and it was found that the variability (the amplitude of the oscillation in fuel flow at a frequency of 0.016 Hz) increased as pressure drop increased, and decreased as the gas flow rate in the transfer line increased. These observations are consistent with the studies performed on the mean flow of pulverized fuel from a hopper in a pneumatic conveying system. A model is proposed to account for the fuel flow variability over time, which can be used with the Sprouse and Schuman model and a reduced order model to determine the influence of fuel flow variability on gasification performance.

The pneumatic conveying system used demonstrated a significant amount of variability at higher frequencies in the range that was measured. The higher frequencies were shown to be associated with measurement error, suggesting that the observed fluctuations in fuel flow are either attributed to the aeration pads, or attributed to error. However, other researchers such as Sprouse *et al.* [53], and experiments performed prior to the installation of the aeration pads on the system used for these experiments, have shown considerable variability as well. The method presented here should be used with more precise flow measurement techniques to determine the true variability of the fuel flow in a pneumatic conveying system.

5. Conclusions and future work

The goal of this thesis was to determine the pneumatic conveying characteristics of pulverized fuels, as well as to determine the jet half-angle of a gas-solid fuel jet, for use in reduced order models with application in entrained flow gasification systems. In summary, the objectives were:

- Develop a pneumatic conveying system for the continuous flow of pulverized fuels, namely lignite, petroleum coke, and biomass, from a fuel supply hopper to an entrained flow gasification unit;
- Determine the influence of the pneumatic conveying parameters of the system (pressure drop, transport gas flow rates, and transport gas injection point) on the flow rate of the pulverized fuels studied;
- Present a mathematical model for the flow rate of pneumatically conveyed pulverized fuels;
- Determine the influence of pneumatic conveying operating parameters on the jet half-angle of a gas-solid system, specifically the entrained flow gasification of pulverized solid fuels;
- Present a mathematical model for the jet half-angle of a gas-solid system;
- Determine the influence of pneumatic conveying operating parameters (pressure drop and gas flow rate) on the variability of the solid flow rate;
- Present a mathematical model for the variability of the solid flow rate of fuel over time.

A pneumatic conveying system was designed to convey pulverized fuels to a pilot-scale entrained flow gasifier. The system was design such that biomass, which was proven to be the most difficult of the three fuels to convey, could be conveyed continuously until the supply was

exhausted. The key system components were: fluidizing gas injection at the bottom of the feed hopper to prevent consolidation while pressurizing the system; sparge gas injection through a tube inserted from the top of the hopper, through the bed of material to prevent consolidation of the material in the bottom conical section of the hopper; aeration pads pulsating transport gas into the hopper on a one-minute cycle to prevent channeling occurring; transfer gas injected into the fuel transfer line (outside of the hopper) to allow for a more direct control of the quantity of gas in the transfer line.

Non-reactive conveying was performed at different conditions to determine the impact of pressure drop, gas injection points, and gas flow rates. The pressure drop was varied from 75 kPa to 240 kPa between the feed hopper and the receiver hopper. The fluidizing gas and sparge gas was varied from 1 kg/h to 15 kg/h, and the transfer gas was varied from 1 kg/h to 8 kg/h. The intensity and frequency of the aeration pads were not varied; they remained at an occurrence of one pulse of ten seconds every one minute, while an approximate flow rate of 3.2 kg/h over the ten second period. For all three fuels, the fuel flow rate increased as the pressure drop was increased, and as the gas flow rates were decreased, with the exception of the fluidizing gas which appeared to have no effect on the fuel flow rate. The influence of these parameters had a reduced effect on the biomass; while the fuel flow rate did increase, it did not increase as significantly as the lignite or petroleum coke.

The Sprouse and Schuman model was shown to fit the experimental data. The model is based on a momentum balance of the solid and gas phases in the transfer line. There are two parameters in the model that must be determined by best fit: the coefficient of hopper discharge and the coefficient of wall friction. The coefficient of hopper discharge was found to be 0.0878, and is specific to the conveying system used. The coefficient of wall friction is specific to each fuel,

and was found to be 1.18 x 10^{-5} for the biomass, 1.71 x 10^{-6} for the lignite, and 1.76 x 10^{-6} for the petroleum coke. The biomass was shown to have a much greater difficulty to convey than the lignite and petroleum coke, and was shown to be less influenced by changes to the operating parameters. Additionally, SEM images of the biomass show that it is much less uniformly shaped than the other fuels. Considering these factors, it is not surprising that the coefficient of wall friction for the biomass is higher than for the other fuels.

The jet half-angle in an entrained flow gasifier was studied using laser imaging in a non-reactive environment. The jet half-angle was measured at different solid loading ratios (defined as the mass of solids over the mass of gas in the jet core at the nozzle exit) ranging 1-17.3 kg_{solid}/kg_{gas}. The half-angles were shown to increase from 5.6° to 11.3° as the solid loading ratio was decreased, which is consistent with observations made by other researchers. Previous work done on liquid and gas systems show that the jet half-angle increases with the density ratio R, defined as the ratio of the fluid surrounding the jet to the density of the fluid in the jet core. It is shown that the relation holds true for gas-solid systems, in which the density of the jet core is defined as the effective density (the weighted average of the solid and fluid densities).

A model was proposed for the jet half-angle in a gas-solid system based on a simple model for liquid systems proposed by Roy *et al.* [46]. The model was compared to CFD results for hot-flow systems, and was shown to account for the lower jet half-angle expected in reactive systems, emphasizing the influence of the density ratio on the jet half-angle.

An attempt was made to quantify the variability observed in the fuel flow of a pneumatic conveying system. A frequency analysis was performed on the fuel flow rate by applying a Fast-Fourier transform to the time-domain data set, using Origin® 2015. The Peak Analyzer software in Origin® 2015 was also used to determine significant peaks in the frequency-domain resulting

from the analysis. A significant peak was observed at a frequency of 0.016 Hz, which coincides with the frequency of the aeration pads, suggesting that the aeration pads assist in discharge fuel from the hopper. The effect of pressure drop (ranging 90-200 kPa) and gas flow rate (ranging 2.8-7.3 kg/h) on the amplitude of the observed frequency was studied. It was shown that the amplitude increases as the pressure drop increases, and as the gas flow rate in the transfer line decreases. These trends are consistent with observations made regarding the mean fuel flow rate. A model for the variability of fuel flow over time was proposed based on the frequency-domain results of the analysis.

Overall, three models were analyzed herein: a model representing the mean fuel flow rate of a pneumatic conveying system (expanded from Sprouse and Schuman [14]) as a function of operating parameters, notably the pressure drop and gas flow rates; a model representing the half-angle of a gas-solid jet (expanded from Roy *et al*. [46]) as a function of the jet ambient-to-core density ratio, which in turn is depended on the solid loading ratio; and a model representing the variability of fuel flow over time, determined by a frequency analysis on the fuel flow measurements of a pneumatic conveying system.

These models can be used with one another to determine the nested influence of the operating parameters. For instance, the frequency model can be coupled with the half-angle to determine how the jet half-angle can be expected to vary as the operating parameters (pressure drop and gas flow rate) are varied. Additionally, these models can be used with a reduced order model to determine how the operating parameters influence the gasification process. An example of such a case is as follows: an increase of the sparge gas flow rate will influence the mean fuel flow rate, as well as the variability of the fuel flow rate as per the frequency analysis; the change in both gas and solid fuel flow rate will influence the jet half-angle as per the solid loading ratio; all of

these parameters (gas flow rate, solid flow rate, and jet half-angle) will influence the gasifier performance (conversion, yield, temperature profile), which can be calculated using a reduced order model.

Potential future work includes validating the frequency analysis method using more sensitive fuel flow measurement equipment, such that high-frequency low-amplitude peaks can be studied, as well as studying the jet half-angle of a gas-solid stream at high temperatures.

6. References

[1] International Energy Agency, CO2 Emissions from Fuel Combustion, 2012.

[2] H. Rodhe, A comparison of the contribution of various gases to the greenhouse effect., Science. 248 (1990) 1217–1219.

[3] M. Meinshausen, N. Meinshausen, W. Hare, S.C.B. Raper, K. Frieler, R. Knutti, et al., Greenhouse-gas emission targets for limiting global warming to 2 degrees C., Nature. 458 (2009) 1158–1162.

[4] C. Kunze, H. Spliethoff, Assessment of oxy-fuel, pre- and post-combustion-based carbon capture for future IGCC plants, Appl. Energy. 94 (2012) 109–116.

[5] A.S. Bhown, B.C. Freeman, Analysis and status of post-combustion carbon dioxide capture technologies, Environ. Sci. Technol. 45 (2011) 8624–8632.

[6] B.J.P. Buhre, L.K. Elliott, C.D. Sheng, R.P. Gupta, T.F. Wall, Oxy-fuel combustion technology for coal-fired power generation, Prog. Energy Combust. Sci. 31 (2005) 283–307.

[7] C. Higman, M. van der Burgt, Gasification, 2nd ed., Gulf Professional Publishing, Boston, 2008.

[8] J.J. Hernández, G. Aranda-Almansa, A. Bula, Gasification of biomass wastes in an entrained flow gasifier: Effect of the particle size and the residence time, Fuel Process. Technol. 91 (2010) 681–692.

[9] C. Chen, M. Horio, T. Kojima, Numerical simulation of entrained flow coal gasifiers. Part I: Modeling of coal gasification in an entrained flow gasifier, Chem. Eng. Sci. 55

(2000) 3861–3874.

[10] V. Kirubakaran, V. Sivaramakrishnan, R. Nalini, T. Sekar, M. Premalatha, P. Subramanian, A review on gasification of biomass, Renew. Sustain. Energy Rev. 13 (2009) 179–186.

[11] J.S. Brar, K. Singh, J. Wang, S. Kumar, Cogasification of Coal and Biomass: A Review, Int. J. For. Res. 2012 (2012) 1–10.

[12] B.N. Murthy, A.N. Sawarkar, N. a. Deshmukh, T. Mathew, J.B. Joshi, Petroleum coke gasification: A review, Can. J. Chem. Eng. 92 (2014) 441–468.

[13] E.H. Chui, a. J. Majeski, D.Y. Lu, R. Hughes, H. Gao, D.J. McCalden, et al., Simulation of entrained flow coal gasification, Energy Procedia. 1 (2009) 503–509.

[14] K.M. Sprouse, M.D. Schuman, Dense-phase feeding of pulverized coal in uniform plug flow, AIChE J. 29 (1983) 1000–1007.

[15] D. Geldart, S.J. Ling, Dense phase conveying of fine coal at high total pressures, Powder Technol. 62 (1990) 243–252.

[16] A. Bansal, S.S. Mallick, P.W. Wypych, Investigating Straight-Pipe Pneumatic Conveying Characteristics for Fluidized Dense-Phase Pneumatic Conveying, Part. Sci. Technol. 31 (2013) 348–356.

[17] G. Setia, S.S. Mallick, P.W. Wypych, On improving solid friction factor modeling for fluidized dense-phase pneumatic conveying systems, Powder Technol. 257 (2014) 88–103.

[18] W. Huang, X. Gong, X. Guo, Z. Dai, H. Liu, L. Zheng, et al., Discharge characteristics of

cohesive fine coal from aerated hopper, Powder Technol. 194 (2009) 126–131.

[19] M.H. Sahraei, R. Yandon, M. a. Duchesne, R.W. Hughes, L. a. Ricardez-Sandoval, Parametric Analysis Using a Reactor Network Model for Petroleum Coke Gasification, Energy & Fuels. 29 (2015) 7681–7688.

[20] R.F.D. Monaghan, A.F. Ghoniem, A dynamic reduced order model for simulating entrained flow gasifiers: Part I: Model development and description, Fuel. 91 (2012) 61–80.

[21] D. Fleckhaus, K. Hishida, M. Maeda, Effect of laden solid particles on the turbulent flow structure of a round free jet, Exp. Fluids. 5 (1987) 323–333.

[22] R.S. Barlow, Two-phase velocity measurements in dense particle-laden jets, Exp. Fluids. 104 (1990) 93–104.

[23] X. Guo, Z. Dai, X. Gong, X. Chen, H. Liu, F. Wang, et al., Performance of an entrained-flow gasification technology of pulverized coal in pilot-scale plant, Fuel Process. Technol. 88 (2007) 451–459.

[24] J. Fermoso, B. Arias, M.G. Plaza, C. Pevida, F. Rubiera, J.J. Pis, et al., High-pressure co-gasification of coal with biomass and petroleum coke, Fuel Process. Technol. 90 (2009) 926–932.

[25] J. Wang, E.J. Anthony, J.C. Abanades, Clean and efficient use of petroleum coke for combustion and power generation, Fuel. 83 (2004) 1341–1348.

[26] G.E. Klinzing, F. Rizk, R. Marcus, L.S. Leung, Pneumatic Conveying of Solids, Springer Netherlands, Dordrecht, 2010.

[27] D. Mills, Pneumatic conveying design guide, 2004.

[28] A. Van der Drift, H. Boerrigter, B. Coda, Entrained flow gasification of biomass, Energy Centre of the Netherlands, 2004.

[29] D. Geldart, Types of gas fluidization, Powder Technol. 7 (1973) 285–292.

[30] J. Dai, J.R. Grace, Biomass granular screw feeding: An experimental investigation, Biomass and Bioenergy. 35 (2011) 942–955.

[31] H.-Y. Xie, D. Geldart, Fluidization of FCC powders in the bubble-free regime: effect of types of gases and temperature, Int. J. Multiph. Flow. 82 (1995) 269–277.

[32] H. Lu, X. Guo, S. Tao, X. Gong, A further study on effect of gas type on pulverized coal discharge, Powder Technol. 281 (2015) 193–199.

[33] S.-P. Shi, S.E. Zitney, M. Shahnam, M. Syamlal, W.A. Rogers, Modelling coal gasification with CFD and discrete phase method, J. Energy Inst. 79 (2006) 217–221.

[34] D.F. Fletcher, B.S. Haynes, F.C. Christo, S.D. Joseph, A CFD based combustion model of an entrained flow biomass gasifier, Appl. Math. Model. 24 (2000) 165–182.

[35] M.H. Sahraei, M. a. Duchesne, R. Yandon, A. Majeski, R.W. Hughes, L. a. Ricardez-Sandoval, Reduced order modeling of a short-residence time gasifier, Fuel. 161 (2015) 222–232.

[36] R.F.D. Monaghan, A.F. Ghoniem, Dynamic Reduced Order Modeling of Entrained Flow Gasifiers, (2010) 300.

[37] P.O. Hedman, L.D. Smoot, Particle-gas dispersion effects in confined coaxial jets, AIChE J. 21 (1975) 372–379.

[38] D. Modarress, H. Tan, S. Elghobashi, Two-component LDA measurement in a two-phase turbulent jet, AIAA J. 22 (1984) 624–630.

[39] J. Zhang, L. Zhou, Particle behaviors in a pulverized coal-fired sudden-expansion combustor with coaxial jets, Fuel. 80 (2001) 289–299.

[40] T.G. Almeida, F. a. Jaberi, Large-eddy simulation of a dispersed particle-laden turbulent round jet, Int. J. Heat Mass Transf. 51 (2008) 683–695.

[41] M. Sijercic, S. Belosevic, Z. Stevanovic, Simulation of free turbulent particle-laden jet using Reynolds-stress gas turbulence model, Appl. Math. Model. 31 (2007) 1001–1014.

[42] H. Liu, W. Cao, J. Xu, W. Li, X. Guo, Z. Sun, Characterization of the granular jet in a coaxial gas stream, Powder Technol. 225 (2012) 206–213.

[43] W.E. Ranz, Some experiments on orifice sprays, Can. J. Chem. Eng. 36 (1958) 175–181.

[44] R.D. Reitz, R.D. Reitz, F. V Bracco, F. V Bracco, Ultra-high-speed filming of atomizing jets, Phys. Fluids. 22 (1979) 1054–1064.

[45] K.-J. Wu, C.-C. Su, R.L. Steinberger, D. a. Santavicca, F. V. Bracco, Measurements of the Spray Angle of Atomizing Jets, J. Fluids Eng. 105 (1983) 406.

[46] A. Roy, C. Segal, C. Joly, Spreading Angle and Core Length Analysis of Supercritical Jets, AIAA J. 51 (2013) 2009–2014.

[47] N. a. Chigier, A. Chervinsky, Experimental Investigation of Swirling Vortex Motion in Jets, J. Appl. Mech. 34 (1967) 443–451.

[48] F.P. Ricou, D.B. Spalding, Measurements of entrainment by axisymmetrical turbulent jets, J. Fluid Mech. 11 (1961) 21–32.

[49] J.M. Beér, N.A. Chigier, Combustion Aerodynamics, John Wiley & Sons, New York, 1972.

[50] M. Rhodes, Introduction to Particle Technology, 1993.

[51] F.T. Kus, M.A. Duchesne, S. Champagne, R.W. Hughes, D.Y. Lu, A. Macchi, et al., Pressurized pneumatic conveying of pulverized fuels for entrained flow gasification, Powder Technol. 287 (2016) 403–411.

[52] S.G. Daviault, O.B. Ramadan, E. a. Matida, P.M. Hughes, R. Hughes, Atomization performance of petroleum coke and coal water slurries from a twin fluid atomizer, Fuel. 98 (2012) 183–193.

[53] K.M. Sprouse, D.R. Matthews, G.F. Weber, Dry Coal Feed System and Multi-Element Injector Test Report, 2008.

[54] F. Johnsson, R.C. Zijerveld, J.C. Schouten, C.M. Van Den Bleek, B. Leckner, Characterization of fluidization regimes by time-series analysis of pressure fluctuations, Int. J. Multiph. Flow. 26 (2000) 663–715.

[55] J. Xu, X. Bao, W. Wei, G. Shi, S. Shen, H.T. Bi, et al., Statistical and frequency analysis of pressure fluctuations in spouted beds, Powder Technol. 140 (2004) 141–154.

[56] J. van der Schaaf, J.R. van Ommen, F. Takens, J.C. Schouten, C.M. van den Bleek, Similarity between chaos analysis and frequency analysis of pressure fluctuations in fluidized beds, Chem. Eng. Sci. 59 (2004) 1829–1840.

[57] J.R. Van Ommen, S. Sasic, J. Van der Schaaf, S. Gheorghiu, F. Johnsson, M.O. Coppens, Time-series analysis of pressure fluctuations in gas-solid fluidized beds - A review, Int. J.

Multiph. Flow. 37 (2011) 403–428.

[58] M.R. Portnoff, Time-Frequency Representation of digital Signals, IEEE Trans. Acoust. Speech Signal Process. ASSP. 28 (1980) 55–69.

[59] I. Daubechies, The wavelet transform, time-frequency localization and signal analysis, IEEE Trans. Inf. Theory. 36 (1990).

[60] L. Stankovic, Method for time-frequency analysis, IEEE Trans. Signal Process. 42 (1994) 225–229.